Pharmacophore-based design of phenyl-[hydroxycyclohexyl] cycloalkyl-carboxamide mitofusin activators with improved neuronal activity

Xiawei Dang[1,2], **Sidney B. Williams**[3], **Sriram Devanathan**[3], **Antonietta Franco**[2], **Lijun Fu**[4], **Peter R. Bernstein**[5], **Daniel Walters**[6], **Gerald W Dorn II**[2,3,*]

[1]Department of Cardiology, The First Affiliated Hospital of Xi'an Jiao Tong University, Xi'an, Shaanxi 710061, China

[2]Department of Internal Medicine, Washington University School of Medicine, St. Louis, Missouri 63110, USA

[3]Mitochondria in Motion, Inc., 4340 Duncan Avenue, Suite 216, St. Louis, Missouri 63110, USA

[4]WuXi AppTec Co., Ltd. 666 Gaoxin Rd, East Lake High-tech Development Zone, Wuhan, Hubei 430075, China

***Correspondence to:** Gerald W. Dorn II, MD, Philip and Sima K. Needleman Professor, Washington University Center for Pharmacogenomics, 660 S Euclid Ave. Campus Box 8220, St. Louis, MO 63110, Phone: 314 362-4892. Fax 314 362-8844., gdorn@wustl.edu.

Supporting Information

Figure S1 (Dose response curves and EC$_{50}$ values of **1-6**); Figure S2 (^{1}H-NMR spectrum of intermediate **5C**); Figure S3 (Characteristics of **9** and **10** starting material); Figure S4 (Crystalization of **9** and **10** for single crystal X-ray diffraction studies); Figure S5 (Structural modeling of positions for human MFN2 amino acids mimicked by small molecule mitofusin activators); Figure S6 (HPLC, ^{1}H NMR and ^{13}C NMR chromatography of **5**); Figure S7 (HPLC, ^{1}H NMR and ^{13}C NMR chromatography of **6**); Figure S8 (HPLC, ^{1}H NMR and ^{13}C NMR chromatography of **7**); Figure S9 (HPLC, ^{1}H NMR and ^{13}C NMR chromatography of **8**); Figure S10. HPLC and ^{1}H NMR chromatography of **9;** Figure S11. HPLC and ^{1}H NMR chromatography of **10;** Figure S12. HPLC and ^{1}H NMR chromatography of **11;** Figure S13. HPLC and ^{1}H NMR chromatography of **12;** Figure S14. HPLC and ^{1}H NMR chromatography of **13;** Figure S15 (SFC, ^{1}H NMR and ^{13}C NMR chromatography of **5A** and **5B**); Figure S16. HPLC and ^{1}H NMR chromatography of **14A** and **14B**. Table S1. Solvents used in slow cooling experiments. Table S2. Parameters used in X-ray powder diffraction. Table S3. Parameters used in thermogravimetric analysis (TGA) and differential scanning calorimetry (DSC). Table S4. Summary of slow evaporation experiments. Table S5. Summary of layer diffusion experiments. Molecular formula string for all the final compounds (CSV). 3D PDB files for Figure S5 (PDB).

Accession Codes

CCDC 2057833-2057834 contain the supplementary crystallographic data for this paper. These data can be obtained free of charge via www.ccdc.cam.ac.uk/data_request/cif, or by emailing data_request@ccdc.cam.ac.uk, or by contacting The Cambridge Crystallographic Data Centre, 12 Union Road, Cambridge CB2 1EZ, UK; fax: +44 1223 336033.

PDB ID Code

Human Mfn1 (PDB ID: 5GNS) and Arabidopsis thaliana dynamin-related protein (PDB ID: 3T34) were used to computationally model human Mfn2 closed configuration based on structural homology has been described previously ([15]). And this hypothetical human Mfn2 structure and hMFN2 found in the protein database (PDB; code 6JFM) were used for molecular modeling with compound **14A** and **14B**, authors will release the atomic coordinates and experimental data upon article publication.

[5]PharmaB LLC, 50 S. 16th Street, Unit 5201, Philadelphia, PA 19102, USA

[6]Crystal Pharmatech Inc., 3000 Eastpark Blvd., Ste 500B, Cranbury, New Jersey 08512, USA

Abstract

Mitochondrial fragmentation from defective fusion or unopposed fission contributes to many neurodegenerative diseases. Small molecule mitofusin activators reverse mitochondrial fragmentation *in vitro,* promising a novel therapeutic approach. The first-in-class mitofusin activator, **2**, has a short plasma $t_{1/2}$ and limited neurological system bioavailability, conferring "burst activation". Here, pharmacophore-based rational redesign generated analogs of **2** incorporating cycloalkyl linker groups. A cyclopropyl-containing linker, **5**, improved plasma and brain $t_{1/2}$, increased nervous system bioavailability, and prolonged neuron pharmacodynamic effects. Functional and single crystal X-ray diffraction studies of stereoisomeric analogs of **5** containing sulfur as a "heavy atom", **14A** and **14B,** showed that **5** biological activity resides in the t*rans*-R/R configuration, **5B**. Structural analysis revealed stereoselective interactions of **5** associated with its mimicry of MFN2 Val372, Met376 and His380 side chains. Modification of murine ALS phenotypes *in vitro* and *in vivo* support advancement of **5B** for neurological conditions that may benefit from sustained mitofusin activation.

Graphical Abstract
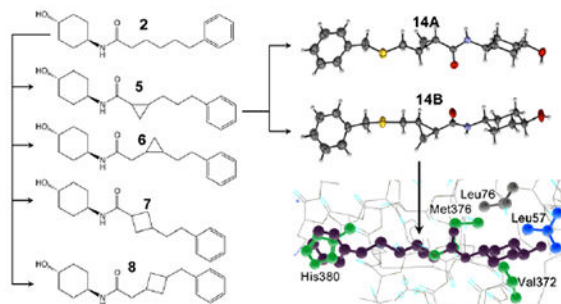
INTRODUCTION

Mitochondrial fragmentation caused by an imbalance between mitochondria fusion and fission is a common cause of, and contributor to, neurodegenerative diseases ([1, 2]). Mitochondrial fusion is initiated by outer mitochondrial membrane-embedded mitofusin (MFN) proteins whose extra-organelle domains extend across cytosolic space to interact with counterparts on neighboring mitochondria, physically linking organelles via MFN-MFN dimers/oligomers ([3]). Mitofusins subsequently induce outer mitochondrial membrane fusion through a process requiring catalytic GTPase activity ([4–6]). Multiple mitofusin 2 (*MFN2*) mutations, most frequently located within the MFN2 GTPase domain, are implicated in a rare untreatable childhood sensory-motor neuropathy, Charcot-Marie-Tooth (CMT) disease type 2A ([7, 8]). Defects in mitofusin function or expression are also described in other neurodegenerative conditions, including experimental amyotrophic lateral sclerosis ([9]) and clinical Huntington's disease ([10]). For these reasons mitofusins are attractive drug targets ([11]).

Developing a pharmaceutically acceptable activator of mitofusins to enhance mitochondrial fusion was challenging. The anti-rheumatic drug leflunomide was identified as a transcriptional enhancer of mitofusin mRNA expression, but effective concentrations are high (10-50 μM) [12]. A putative small molecule mitofusin activator, 4-chloro-2-(1-(2-(2,4,6-trichlorophenyl) hydrazineylidene) ethyl)phenol, was detected by high-throughput screening for fusogenic compounds, but with an EC_{50} of 4-5 μM it also has limited utility except as a research tool [13]. Franco, et al designed an 18 amino acid cell-permeant mitofusin activating peptide modified from hMFN2 amino acids 367-384 that could be introduced into cells using amino terminal TAT_{47-57} conjugation [14]. This peptide activates mitofusins by competing for and disrupting intramolecular peptide-peptide bonds enforcing the closed (inactive) mitofusin protein conformation and has greater potency for mitofusin stimulation than the above compounds (EC_{50} ~0.3 μM). However, as peptides their therapeutic utility in clinical disease seems limited. Thus, Rocha et al [15] developed small triazolurea-containing molecules, like **1,** that potently induce mitochondrial fusion (EC_{50} ~5 nM) by mimicking function-critical amino acids of the Franco activator peptide. Unfortunately, mitofusin activators with this chemical structure proved incompatible with *in vivo* use [16].

Phenylhexanamide mitofusin activators possessing drug-like properties were recently described [16]. The lead compound of this chemical series (**2**) demonstrated *in vivo* engagement of neuronal mitochondria after intravenous administration; its daily intramuscular administration reversed neuromuscular degeneration in a mouse model of CMT2A [17]. However, this compound has a short half-life in mouse plasma ($t_{1/2}$ 1.1h) and brain ($t_{1/2}$ 1.06h), properties most suitable for "burst activation" of mitofusins [17]. We posited that mitofusin activators having more prolonged presence in the central nervous system could have greater therapeutic utility in other neurodegenerative conditions.

Here, we extended mitofusin activator design by employing the previously described pharmacophore-based strategy [16]. We considered that structurally more rigid and metabolically stable compounds resulting from introduction of cycloalkyl modifications into the hexanamide linker [18–21] might have greater engagement of neuronal mitochondria. In particular, introduction of cyclopropyl rings into different compounds has increased potency, selectivity, oral bioavailability, metabolic and chemical stability, or neurological system exposure. Relevant to our pharmacophore-based design strategy, cyclopropyl rings have been employed to restrict the conformation of the serotonin and norepinephrine re-uptake inhibitor Z-Milnacipran and the monoamine oxidase inhibitor Tranylcypramine [21]. Here, a pre-clinical lead compound having a linker cyclopropyl group, **5**, exhibited potent stereospecific mitofusin activation and longer plasma and brain $t_{1/2}$ than **2**. Single crystal X-ray crystallography of **5** sulfide analogs [**14A** and **14B**] revealed that the (*trans*-R,R) enantiomer uniquely conferred mitofusin agonist activity. The crystal structure moiety distances and hydrogen bonding characteristics mimicked those of function-critical amino acid side chains within the precursor mitofusin agonist peptide, consistent with the pharmacophore model. *In vitro* and *in vivo* proof of concept studies with **5B** in murine amyotrophic lateral sclerosis (ALS) support its clinical development for neurodegenerative diseases linked to mitochondrial dysfunction.

RESULTS AND DISCUSSION

Rational re-design of mitofusin activators.

Prototype triazolurea (**1**) and phenylhexanamide (**2**) mitofusin agonists share the general structure of a substituted cyclohexyl group (R1) connected to an aromatic moiety (R2) by urea- or carboxamide-containing alkyl linkers (Figure 1A). The linker promotes optimal spacing between R1 and R2, which according to the pharmacophore model ([15]), respectively mimic human MFN2 His380 and Met376/Val372. The linker can be a source of conformational plasticity, but the published pharmacophore model and reported structure-activity relationships ([15, 16]) suggest that mitofusin activators can be modified to retain biological activity if R1-R2 separation distance is conserved. Indeed, deletion of one (**3**) or two (**4**) carbons from the **2** linker largely abrogated mitofusin activation measured as the ability to promote mitochondrial fusion (increased aspect ratio: length/width) (Figure 1B). Accordingly, we posited that introduction of small cycloalkyl linker groups that do not alter R1-R2 distance could both stabilize the molecule and enhance passive membrane permeability reported to correlate with blood brain barrier penetration ([16]). Structures and characteristics of parent **2** and nine cycloalkyl linker analogs are shown in Figure 2.

In vitro characterization of mitofusin activators with cycloalkyl linkers.

To gauge how pharmacophore modeling conformed to reality, mitofusin activation by **5-13** was compared using the mitochondrial elongation fusogenicity assay in MFN2-deficient cells ([14–16]). Because the *trans*-cyclohexanol stereoisomer of parent **2** was biologically active whereas the corresponding *cis*-analog was not ([16]), **5-13** were each synthesized as *trans* stereoisomers at this position. The cyclopropyl analogs, **5** and **6**, were potent mitofusin activators having EC_{50} values for mitochondrial elongation similar to parent **2**, i.e. ~5-6 nM (Table 1). There was no clear benefit to increasing the size of linker cycloalkyl groups, which increased PAMPA Pe, but also increased instability in the mouse liver microsomal assay (Table 1, Figure S1).

In vivo pharmacokinetic properties of 5.

Among the newly synthesized and characterized cycloalkyl linker analogs of **2**, *in vitro* characteristics of **5** appeared pharmaceutically most favorable. Therefore, *in vivo* PK studies of **5** were undertaken in mice, the species in which all previous PK studies of mitofusin activators have been performed ([16]). Plasma **5** levels were measured at increasing times after administration of single 10 mg/kg intravenous (IV) doses. Compared to published values for **2** ([16]), **5** had ~50% longer plasma elimination $t_{1/2}$ and proportionally greater tissue distribution (Vdss) values, with correspondingly reduced peak plasma and AUC levels (Table 2).

Fusogenicity and mitofusin-interactions of 5 are stereoisomer-specific.

Because only the *trans*-cyclohexanol stereoisomer of **2** has biological activity ([16]), **5-13** were synthesized as *trans*-isomers at the cyclohexanol group. However, the linker cyclopropyl group in **5** creates additional chiral centers to either side, with 4 possible stereoisomers (Figure 3, **left**). Chiral separation of **5** by supercritical fluid chromatography (SFC-H)

identified only two isomers, designated -A and -B for the faster and slower eluting forms, respectively (Figure 3, **right**). Proton NMR of synthetic intermediate **5C** revealed a coupling constant of ~19 Hz for the olefin proton at 6.75 ppm, indicating trans-olefin geometry (Figure S2). In agreement with expectations based on known reaction mechanism, the product of the Corey-Chaykovsky reaction leading to **5** (**Synthetic** Scheme 2) contained only two isomers: *trans*-R,R and S,S (Figure 3).

Mitofusin-stimulating activities of **5A** and **5B** were compared by assaying their effects on mitochondrial elongation and polarization status in Mfn1-null (i.e. expressing Mfn2 alone) or Mfn2-null (i.e. expressing Mfn1 only) murine embryonic fibroblasts (Figure 4). The prototype triazolurea mitofusin activator, **1**, was assayed in parallel as a historical comparator. There was little effect produced by **5A** (1 μM, 48 hours) on either outcome. By comparison, **5B** was equipotent with **1** in cells expressing either Mfn1 or Mfn2. Thus, **5B** is a potent mitofusin activator.

We tested **5A** and **5B** interactions with MFN2 protein using a previously described FRET assay that measures MFN2 conformational changes provoked by mitofusin activators [15–17]. Please note that FRET assays were performed on isolated mitochondria, whereas assessments of mitochondrial elongation were performed in intact cells. A high compound concentration (1 uM) was employed to test whether inactivity of enantiomer **5A** to promote mitochondrial elongation in cells corresponded with FRET inactivity for *in vitro* target engagement. As shown in Figure 5, 5B had the same effect on MFN2 conformation previously described for mitofusin activators **1** [15] and **2** [16]) i.e. it decreased the FRET signal, reflecting separation of the N-terminal mCerulean and C-terminal mVenus fluorophores after unfolding of the protein into its active conformation. By comparison, **5A** did not decrease the FRET signal. Thus, **5A** did not conformationally activate MFN2.

X-ray diffraction reveals enantiomeric structures of 5A and 5B.

Although **5A** and **5B** were determined to be the *trans*-cyclopropyl stereoisomers (*vide supra*), it was not possible to assign R,R vs S,S structures to the stereoisoforms. Thus, we synthesized heavier sulfide analogs of **5A** and **5B** for X-ray diffraction studies, designated **14A** and **14B** respectively (Figure 6A). Like their respective parents, **14B** potently stimulated mitochondrial elongation in Mfn2 null fibroblasts, whereas **14A** had poor biologically activity (Figure 6B).

The X-ray powder diffraction patterns and small rod-like crystal morphologies under polarized light microscopy of **14A** and **14B** were similar (Figure S3). Crystals used for single-crystal x-ray diffraction (SCXRD) for **14A** were obtained by slow evaporation in acetonitrile (Figure S4A), and for **14B** by slow evaporation in ethyl acetate (Figure S4B). As anticipated from studies of synthetic intermediates of **5** (see Figure 3), the resulting crystal structures showed that the two compounds are enantiomers, with **14B** displaying {R,R} chirality.

Crystalline structures of **14A** and **14B** displayed no disorder. The asymmetric unit cells contained one molecule of the compound with no solvent molecules present (Figure 7A). Indeed, crystals with identical morphology readily formed out of multiple solvent systems

(Table S1). The packing diagram (Figure 7B) and hydrogen bonding network between **14B** molecules connecting in two directions (Figure 7C) further support absence of solvent molecules. Thus, **14B** molecules form a pseudo-polymeric structure connected by the amide moieties near the center of the molecule. The carbonyl oxygen (O10) forms strong hydrogen bonding interactions with the hydrogens of adjacent molecules' amide nitrogen (N8).

The hydrogen bonding distance measured by the donor-acceptor distance is 2.887 Å. This contact deviates only slightly from the idealized hydrogen geometry as measured by linearity including the idealized H8A across the O10-N8 angle (171.31°). A second hydrogen bonding interaction dimerizes these pseudo-polymeric structures across the terminal alcohol (O1) with a donor-acceptor distance of 2.745 Å, reflecting an even stronger interaction. This is likely the consequence of every involved alcohol being both donor and acceptor, polarizing each oxygen involved. The resulting zig-zag formation and O-O-O angle of 130.72° is conducive to a trigonal planar type interaction.

Bonds within the **14B** cyclopropyl moiety are slightly uneven: the longest interaction is the backbone C11-C13 bond (1.515 Å), while the adjoining bonds are asymmetrical, with a longer bond on the carbon alpha to the electropositive amide carbon (C11-C12, 1.513 Å) and a shorter bond on the carbon beta to the electron-donating sulfur (C13-C12, 1.484 Å). The molecule as a whole, if measured across the two hydrogen atoms idealized upon the two farthest atoms, is 18.415 Å in length. Simulation of the mimicked environment for **14A** and **14B** within hMFN2 is depicted in Figure 8. Positions of human MFN2 amino acids His380, Met376 and Val372 emulated by small molecule mitofusin activators according to the pharmacophore representation ([15, 16]) were modelled according to available protein structural information (Figure S5). Compared to **14B**, **14A** has increased overlap with Leu57. In order for the amide carbonyl to occupy a space similar to Met376, the trans (1r,4r)-4-hydroxycyclohexyl-1-amino group is oriented in such a way that it causes improbable overlap with Leu57. This steric crowding is likely to interfere in the ability of **14A** to interact with the proposed adjacent peptide. The direction of rotation with respect to the phenyl moiety caused by the {R,R} cyclopropyl bridging group in **14B** better accommodates and avoids this critical steric hindrance.

Improved nervous system accumulation of 5B.

Because a potential clinical application of small molecule peptidomimetic mitofusin activators is neurological disorders ([15, 17]), **5B** levels were measured in plasma and brain tissue at increasing times after a single 50 mg/kg oral dose. Plasma pharmacokinetics after oral **5B** administration were similar to those of the **5** isomeric mixture given at an identical dose and route in the same vehicle (10% DMSO, 90% [30% HP-b-CD]): t_{max} for both was 0.5h, $t_{1/2}$ was 2.83h and 3.02h respectively, and mean tissue residence times (MRT) were 3.96h and 3.58h respectively (Table 3; compare with **5** values in Table 2) (Figure 9A). The calculated brain/plasma partition coefficient (AUC_{brain}/AUC_{plasma}; Table 3) was 39.4%, i.e. ~4 fold greater than previously reported for **2** ([16]).

The normal central nervous system (brain and spinal cord) is protected by a semipermeable blood brain barrier (BBB) that impedes non-selective solute transport into the cerebrospinal

fluid. The blood nerve barrier (BNB) serves an analogous function for peripheral nerves ([22]), but is uniquely permeable at dorsal root ganglia (DRG) that contain peripheral sensory nerve bodies ([23]). This raised the possibility that small hydrophobic molecules like **5B** can gain access to peripheral nerves through DRGs and be concentrated therein, with therapeutic implications for treating neuropathies. Accordingly, **5B** levels were compared in brain and spinal cord (parts of the central nervous system protected by the BBB) and both sciatic nerves (large peripheral nerves innervating the lower limbs that carry sensory neurons originating in DRGs). As reported in Table 3 and depicted in Figure 9B, 5B C_{max}, AUC, $t_{1/2}$, and mean residence time (MRT) were similar in all three neurological tissues. Indeed, the variance between the left and right sciatic nerves and the central and peripheral nervous systems was similar. These results do not indicate a meaningful effect of "leaky" DRG BNBs on peripheral nerve levels of this mitofusin activator.

The above results suggested that **5B** might exhibit favorable nervous system pharmacodynamics. Previous studies of mitofusin activators measured disease-relevant pharmacodynamic effects as reversal of mitochondrial dysmotility in mouse disease model sciatic nerve axons ([15, 17]) (Figure 10A). Peak mitochondrial motility after "burst" mitofusin activation with **2** reportedly occurred 4 hours after administration and was completely extinguished after 24 hours. By contrast, peak mitochondrial motility after oral administration of **5B** occurred at 12 hours, and benefits were maintained for greater than 24 hours (Figure 10A–10C). Perhaps as a consequence of these favorable pharmacokinetic and pharmacodynamic properties, **5** partially ameliorated neuromuscular dysfunction in murine amyotrophic lateral sclerosis caused by a mutation of superoxide dismutase 1 (SOD1; [24]), whereas **2** showed no significant benefit (Figure 10D).

Stimulation of mitochondrial motility in murine ALS by **5** was delayed in onset, and of longer than expected duration, based on its plasma (and brain, *vide infra*) levels (Figure 10B). This finding is consistent with the idea that facilitating mitochondrial motility is an indirect effect of mitofusins, mediated via their interactions with Miro proteins that couple mitochondria to the Milton/Trak-dynein/kinesin transport apparatus ([26, 27]). Mitofusin regulation of mitochondrial fusion, motility and mitophagy is mediated by mitofusin interactions with different effector proteins ([28]). It seems likely that mitofusin recruitment of Miro proteins to function-critical subcellular domains or an essential multi-molecular complex is the mechanism by which it facilitates mitochondrial coupling to the subcellular transport apparatus. Both Miro recruitment upon mitofusin activation, and its restoration to baseline after mitofusin inactivation, would take time. This can explain the observed temporal discontinuity between mitofusin activator pharmacokinetics and pharmacodynamics.

Together, the above results support superiority of **5** over **2** for extended pharmacodynamic effects and potential therapeutic value in experimental ALS. To better understand the underlying mechanisms we performed a side-by-side comparison of **5B** and **2** plasma and brain pharmacokinetics. For these comparative studies the two compounds were administered at the same dose (50 mg/kg) and route (oral gavage), and using the same vehicle (5 mg/ml in 30% SBE-bCD). As shown in Figure 11 and Table 4, greater brain

bioavailability (total and free AUCs) and longer plasma and brain $t_{1/2}$s and MRTs were exhibited by **5B**.

Chemistry.

Synthesis of **1** and **2** was previously described ([15, 16]). Synthesis of novel compounds **3-14** was accomplished as outlined in Schemes 1–5. **3** and **4** were formed by coupling of commercially available trans-4-aminocyclohexan-1-ol with 5-phenylpentanoic acid or 4-phenylpentanoic acid, as shown in Scheme 1.

Scheme 2 includes compounds **5, 6** and **14**. Compounds **5,** and **14** were synthesized by similar procedures, but with the replacement of intermediate 5b with the sulfide **14b**. For compounds **5** and **14**, the last two steps d and e, to the acid hydrolysis and amide condensation were accomplished by normal conditions from compounds **5d,** and **14d**. These were obtained from Corey-Chaykovsky cyclopropanation reaction from compounds **5c** and **14c**. In turn, they were obtained from Wittig coupling with compounds **5b** and **14b**. Compound **5b** was formed by oxidation of **5a**. The sequence for compound **6** was similar but had some distinct differences. The aldehyde **6a** needed for coupling with the Wittig reagent was commercially available. Following similar cyclopropanation of **6b** the ester **6c** was reduced to afford alcohol **6d**, which was elongated via sequential formation of the chloride **6e**, followed by cyanation to yield **6f**. Hydrolysis of nitrile **6f** yielded the acid **6g** needed for the final amide coupling step, affording **6**.

7 and **8** were synthesized as shown in Scheme 3. Preparation of **7** commenced with commercially available bromide **7a**, which was converted to the Wittig reagent **7b** via reaction with Triphenylphosphine. Reaction of **7b** via treatment with sodium t-butoxide afforded the intermediate ylide which was coupled with Ethyl 3-oxocyclobutane-1-carboxylate to afford **7c**. This intermediate was converted to the final drug candidate **7**, by hydrolysis of the ester to an intermediate acid followed b amide formation under standard conditions. Preparation of **8** began by formation of **8b** via zinc-copper mediated coupling of trichloracetylchloride with 2-Propen-1-ylbenzene **8a**. Removal of the chlorines by treatment with zinc in acetate acid followed by Wittig coupling afforded intermediate **8c** which was converted to **8** similarly to **7c** to **7**.

9 and **10** were synthesized as shown in Scheme 4. Compound **9** was synthesized starting with commercially available diester **9a** via alkaline hydrolysis to obtain acid **9b**, which was reduced by reaction with borane to afford alcohol **9c**. That alcohol was oxidized with Dess-Martin periodinane to yield aldehyde **9d** which was coupled with Wittig reagent **9e** to yield an intermediate olefin that was reduced with Pd/C under H_2 to obtain ester **9f**. This was hydrolyzed to afford acid **9g** that upon coupling with the 4-amino-cyclohexanol afforded **9**. Compound **10** was synthesized starting with commercially available **10a** through the similar procedures with **9d-9** to obtain **10**.

11-13 were synthesized as shown in Scheme 5. Preparation of **11** began with commercially available carboxylic acid **11a** which was reacted Borane-dimethylsulfide to obtain **11b**. Oxidation of **11b** to aldehyde **11c** was effected with pyridine-sulfur trioxide. Which after

coupling with benzyl(triphenyl)phosphonium bromide afforded olefin **11d**. Hydrogenation of this over Pd/C followed by hydrolysis yielded the penultimate acid **11e.** Coupling of which with 4-amino-cyclohexanol afforded the target **11**. Following a similar sequence **12** was synthesized by starting with commercially available 4-formylcyclohexane-1-carboxylic acid (**12a**). Compound (**13**) was made starting with Suzuki coupling of methyl 4-(4,4,5,5-tetramethyl-1,3,2-dioxaborolan-2-yl)cyclohex-3-ene-1-carboxylate (**13a**) with benzylbromide followed by hydrogenation to afford (**13b**). This intermediate was converted to (**13**) similarly to (**11d**) and (**12b**).

Conclusions

In summary, rational re-design of 6-phenylhexanamide mitofusin activators incorporating cycloalkyl-containing linkers generated novel fusogenic compounds having improved pharmaceutical properties. Preclinical lead compound **5**, containing a cyclopropyl group in the linker, exhibited potent, stereo-selective mitofusin activation. Single crystal X-ray diffraction studies conducted with sulfide analogs of **5A** and **5B** showed that MFN2 interactions and biological activity reside exclusively in the *trans*-(R,R) enantiomer. The structural characteristics of **5B** are consistent with mitofusin activation through physico-chemical mimicry of human MFN2 Val372, Met 376 and His380, i.e. the function-critical amino acids in the progenitor mitofusin agonist peptide ([14]) and provide further support for pharmacophore based rational design of small molecule mitofusin activators. Compared to parent compound **2**, **5B** exhibited sustained brain levels, markedly prolonged pharmacodynamic effects, and disease modification in a proof-of-concept study of murine amyotrophic lateral sclerosis. Thus, **5B** is a strong candidate for preclinical evaluation in diseases wherein sustained activation of mitofusin-mediated mitochondrial fusion and transport might counteract neurological degeneration.

Experimental Section

General procedures and Instrumentation

Compounds are at least 95% pure by HPLC (Column: Kinetex C18 LC, 4.6X50 mm, 5um; Mobile phase A: 0.0375% TFA in water (v/v), B: 0.01875% TFA in Acetonitrile (v/v)) run at 50°C with absorbance at 200nM peaks.

LC-MS/MS (ESI) was performed using multiple systems: 1) SHIMADZU LC-MS-2020 with LabSolution V5.72 analysis software, HPLC used a Chromalith@Flash RP-18E 25*2.0MM column ran at 50°C with PDA (220&254nm) detector, acquired data in scan MS Mode (positive mode) with m/z=100-1000 scan range, drying gas (N2) flow: 15 L/min, DL voltage: 120V and Quarry DC voltage: 20V. 2) Agilent 1200/G6110A instrument with AgilentChemStation Rev. B. 04.03 software. HPLC used a Xbridge C18 2.1*50mm, 5um column ran at 40°C with DAD (220nm)/ELSD detector, acquired data in scan MS Mode (positive mode) with m/z=100-1000 scan range, drying gas (N2) flow: 10 L/min, 350°C, nebulizer pressure: 35psi, capillary voltage: 2500V. NMR spectrometry was carried out on Brucker AVANCE NEO 400MHz with 5mm PABBO BB/19F-1H/D Z-GRD probe.

Synthesis and Characterization of Compounds 1-14

Compounds were synthesized and analyzed at WuXi Apptec Co. Ltd. NMR, analytical HPLC and LC-MS were reported previously. All starting reagents not reported are known compounds purchased by WuXi Apptec Co. Ltd from third party suppliers. The synthesis procedure for compounds **1-2** was reported previously ([16]).

N-((1r,4r)-4-hydroxycyclohexyl)-5-phenylpentanamide (3).—To a mixture of trans 4-aminocyclohexan-1-ol (**3a**, 500 mg, 4.34 mmol, 1.00 eq) and 5-phenylpentanoic acid (**3b**, 928 mg, 5.21 mmol, 1.20 eq) in THF (10.0 mL) was added HATU (2.48 g, 6.51 mmol, 1.50 eq), Et3N (1.32 g, 13.0 mmol, 1.81 mL, 3.00 eq) in one portion at 25 °C. The mixture was stirred at 25 °C for 2 hrs. TLC showed the reaction was completed. TLC indicated (Petroleum: Ethyl acetate=3:1) some compound 2a (Rf=0.14) was remained, and one major new spot with larger (Rf=0.29) polarity was detected. The reaction mixture was diluted with H2O 50.0 mL and extracted with Ethyl acetate 60.0 mL (20.0 mL * 3). The combined organic layers were washed with brine 60.0 mL (20.0 mL * 3), dried over [Na2SO4], filtered and concentrated under reduced pressure to give a residue. The crude product was purified by reversed-phase HPLC (0.1% NH3•H2O). **3** (106.02 mg, 0.38 mmol, 8.87% yield) was obtained as a white solid. LC-MS: RT = 0.851 mins, m/z = 276.4 (M+H)+. HPLC: RT = 1.75 mins, 98.7% purity, under 220 nm. SFC: RT = 1.14 mins, ee% = 100%, under 220 nm. 1H NMR: (400 MHz, MeOD) δ 7.25 - 7.22 (m, 2H), 7.16-7.13 (m, 3H), 3.62 – 3.59 (m, 1H), 3.51 - 3.49 (m, 1H), 2.62-2.59 (m, 2H), 2.18 - 2.14 (m, 2H), 1.92 - 1.88 (m, 4H), 1.63 - 1.59 (m, 4H), 1.32-1.27 (m, 4H).

N-((1r,4r)-4-hydroxycyclohexyl)-4-phenylbutanamide (4).—A mixture of trans 4-aminocyclohexan-1-ol (**3a**, 300 mg, 2.60 mmol, 1.00 eq), 4-phenylbutanoic acid (**4b**, 513 mg, 3.13 mmol, 1.20 eq) and Et3N (790 mg, 7.81 mmol, 1.09 mL, 3.00 eq), HATU (1.49 g, 3.91 mmol, 1.50 eq) in THF (10.0 mL) was stirred at 25 °C for 2 hrs. TLC indicated (Petroleum: Ethyl acetate=3:1) some Compound 2 (Rf=0.12) was remained, and one major new spot with larger (Rf=0.26) polarity was detected. The reaction mixture was diluted with H2O 50.0 mL and extracted with Ethyl acetate 60.0 mL (20.0 mL * 3). The combined organic layers were washed with brine 60.0 mL (20.0 mL * 3), dried over [Na2SO4], filtered and concentrated under reduced pressure to give a residue. The crude product was purified by reversed-phase HPLC (0.1% NH3•H2O). **4** (108.64 mg, 0.42 mmol, 15.9% yield) was obtained as a white solid. LC-MS: RT = 0.820 mins, m/z = 262.3 (M+H)+. HPLC: RT = 1.604 mins, 97.2% purity, under 220 nm. SFC: RT = 1.05 mins, ee% = 100%, under 220 nm. 1H NMR (400 MHz, MeOD) δ 7.27 - 7.23 (m, 2H), 7.18-7.15 (m, 3H), 3.61 - 3.60 (m, 1H), 3.53 - 3.50 (m, 1H), 2.62-2.58 (m, 2H), 2.18 - 2.14 (m, 2H), 1.92 - 1.87 (m, 6H), 1.36 - 1.24 (m, 4H).

N-(4-hydroxycyclohexyl)-2-(3-phenylpropyl)cyclopropane-1-carboxamide (5).—To a solution of oxalyl chloride (4.65 g, 36.6 mmol, 3.20 mL, 1.10 *eq*) in DCM (75.0 mL) was cooled to – 55 °C under N₂ atmosphere was added drop-wise a added the solution of DMSO (5.72 g, 73.2 mmol, 5.72 mL, 2.20 *eq*) in DCM (30.0 mL) was, after stirring for 5 min, drop-wise added 4-phenylbutan-1-ol (**5a**, 5.00 g, 33.2 mmol, 5.08 mL, 1.00 *eq*) in DCM (15.0 mL) was added drop-wise, after stirring for 15 min, TEA (16.8 g, 166

mmol, 23.1 mL, 5.00 *eq*) was added, then it was warmed to 25 °C. At that point 100 ml 1 N HCl was added and the suspension was extracted with DCM 200 mL (100 mL * 2). The combined organic layers were washed with water 50 mL, dried over Na_2SO_4, filtered and concentrated to give 4-phenylbutanal (**5b**, 5.00 g). To a solution of **5b** (5.00 g, 33.7 mmol, 9.80 mL, 1.00 *eq*) in THF (50.0 mL) was added *tert*-butyl 2-(triphenyl-λ5-phosphaneylidene)acetate (16.5 g, 43.8 mmol, 1.30 *eq*), stirred at 20 °C for 12 hrs to give *tert*-butyl (*E*)-6-phenylhex-2-enoate (**5c**, 6.00 g, 24.3 mmol, 72.1% yield). To a solution of NaH (1.17 g, 29.2 mmol, 60.0% purity, 1.20 *eq*) in DMSO (30.0 mL) was added dimethylmethanesulfinic iodide (6.43 g, 29.2 mmol, 1.20 *eq*) and the mixture was stirred at 20 °C for 0.5 hr, then added **5c** (6.00 g, 24.3 mmol, 1.00 *eq*) in DMSO (3.00 mL) and stirred at 20 °C for 1 hr to give *tert*-butyl 2-(3-phenylpropyl)cyclopropane-1-carboxylate (**5d,** 2.10 g, 8.07 mmol, 33.1% yield). Added TFA (7.70 g, 67.5 mmol, 5.00 mL, 17.5 *eq*) to a solution of **5d** (1.00 g, 3.84 mmol, 1.00 *eq*) in DCM (5.00 mL), stirred at 25 °C for 15 hrs to give 2-(3-phenylpropyl)cyclopropane-1-carboxylic acid (**3e**, 800 mg). Added EDCI (1.00 g, 5.22 mmol, 1.50 *eq*), HOBt (564 mg, 4.18 mmol, 1.20 *eq*) and DIPEA (1.35 g, 10.4 mmol, 1.82 mL, 3.00 *eq*), 4-aminocyclohexan-1-ol (580 mg, 3.83 mmol, 1.10 *eq,* HCl) to a solution of **5e** (800 mg, 3.48 mmol, 1.00 *eq*) in DMF (8.00 mL) and stirred at 25 °C for 16 hrs. The residue was purified by prep-HPLC (column: Waters Xbridge C18 150*50mm* 10um; mobile phase: [water(10mM NH4HCO3)-ACN];B%: 28%−58%, 11.5min) to give **5** (110 mg, 361 umol, 10.3% yield) as a white solid. **LC-MS:** R_t = 0.904 min, m/z = 302.1 $(M+H)^+$. **HPLC:** R_t = 2.898 min, purity: 98.6%, under 220 nm. ^{13}**C NMR:** (400 MHz MeOD) δ 173.97, 142.27, 127.96, 127.89, 125.31, 69.07, 35.14, 33.45, 32.23, 30.87, 30.24, 21.27, 20.55, 13.04. ^{1}**H NMR:** (400 MHz MeOD) δ 7.27 - 7.24 (m, 2H), 7.18- 7.15 (m, 3H), 3.64 - 3.61 (m, 1H), 3.55 - 3.50 (m, 1H), 2.64 (t, *J* = 8 Hz, 2H), 1.97 - 1.89 (m, 4H), 1.75- 1.73 (m, 2H), 1.36 - 1.04 (m, 8H), 1.29 - 1.27 (m, 1H), 0.59 - 0.57 (m, 1H).

Separation method of 5A and 5B isoforms from 5 mixture isoforms.—Thar 200 preparative SFC (SFC-7) with Column (ChiralPak IG, 30050mm I.D., 10um), Mobile phase: A for CO2 and B for Methanol(0.1%NH3H20); Gradient: B 35%; Flow rate: 200 mL/min; Back pressure: 100 bar Column temperature: 38°C; Wavelength: 220nm; Cycle time: ~4 min; Sample preparation: Compound was dissolved in ~200 ml methanol; Injection: 10 ml per injection. After separation, the fractions were dried off via rotary evaporator at bath temperature 40°C to get the desired isomers. **5A** was the faster eluting isomer by SFC on IG column, and **5B** was the slower eluting isomer. Waters UPC2 analytical SFC (SFC-H) with column (ChiralPak IG, 150×4.6mm I.D., 3μm); Mobile phase: A for CO_2 and B for Methanol (0.05%DEA); Gradient: B 40%; Flow rate: 2.5 mL/min; Back pressure: 100 bar; Column temperature: 35°C; Wavelength: 220nm. **LCMS: 5A**: Rt=2.445 min, m/c=302.2 $(M+H)^{+,}$ **5B**: Rt=2.445 min, m/c=302.2 $(M+H)^+$. **SFC: 5A:** Rt=0.852 min, **5B:** Rt=1.179 min. ^{13}**C NMR: 5A**: (400 MHz MeOD) δ 173.97, 142.27, 127.96, 127.89, 125.31, 69.07, 35.14, 33.46, 32.24, 30.86, 30.24, 21.29, 20.55, 13.05. **5B**: (400 MHz MeOD) δ 173.97, 142.28, 127.96, 127.90, 125.31, 69.07, 35.14, 33.45, 32.24, 30.86, 30.24, 21.29, 20.55, 13.05.

N-(4-hydroxycyclohexyl)-2-(2-phenethylcyclopropyl)acetamide (6).—*Tert*-butyl 2-(triphenyl-λ5-phosphaneylidene)acetate (25.2 g, 67.0 mmol, 1.50 *eq*) to a solution of

3-phenylpropanal (**6a**, 6.00 g, 44.7 mmol, 5.88 mL, 1.00 *eq*) in THF (100 mL) and stirred at 20 °C for 1 hr to give *tert*-butyl (*E*)-5-phenylpent-2-enoate (**6b**, 10.0 g, 42.1 mmol, 94.3% yield).

Dimethylmethanesulfinic iodide (10.0 g, 45.5 mmol, 1.20 *eq*) was added to a solution of NaH (1.82 g, 45.5 mmol, 60.0% purity, 1.20 *eq*) in DMSO (45.0 mL) and the mixture was stirred at 20 °C for 0.5 hr, then **6b** (9.00 g, 37.9 mmol, 1.00 *eq*) in DMSO (5.00 mL) was added and the reaction mixture stirred at 20 °C for 1 hr to give *tert*-butyl 2-phenethylcyclopropane-1-carboxylate (**6c**, 6.00 g, 24.3 mmol, 64.1% yield). LiAlH$_4$ (924 mg, 24.3 mmol, 2.00 *eq*) at 0 °C was added to a solution of **6c** (3.00 g, 12.1 mmol, 1.00 *eq*) in THF (45.0 mL), stirred at 25 °C for 3 hrs, then the reaction mixture was cooled to 0 °C and 1.00 mL water was drop-wise added, then added 1.00 mL 15.0 % NaOH, next 3.00 ml water and warmed to 25 °C, stirred for 15 mins, added 20.0 g MgSO$_4$ and stirred for 15 mins to give (2-phenethylcyclopropyl)methanol (**6d**, 2.00 g, 10.1 mmol, 82.9% yield). A solution of (2-phenethylcyclopropyl)methanol (**6d**, 2.00 g, 10.1 mmol, 1.00 *eq*) and TEA (2.04 g, 20.2 mmol, 2.81 mL, 2.00 *eq*) in CHCl$_3$ (20.0 mL) was cooled to 0 °C and drop-wise added SOCl$_2$ (2.40 g, 20.2 mmol, 1.47 mL, 2.00 *eq*) was added dropwise. The reaction mxture was stirred at 70 °C for 1 hr. The organic phase was separated, the aqueous phase extracted with DCM 40.0 mL (20 mL * 2). The combined organic layers were washed with brine 20.0 mL, dried over Na$_2$SO$_4$, filtered and concentrated. The residue was purified by column chromatography (SiO$_2$, Petroleum ether / Ethyl acetate = 1 / 0, Plate 2, Petroleum ether / Ethyl acetate = 1 / 0,Rf = 0.50) to give (2-(2-(chloromethyl)cyclopropyl)ethyl)benzene (**6e**, 1.80 g, 8.69 mmol, 86.0% yield). Stirred a solution of 2-(2-(chloromethyl)cyclopropyl)ethyl)benzene (**6e**, 1.80 g, 8.69 mmol, 1.00 *eq*) in THF (9.00 mL) and N(nBu)$_4$CN (2.80 g, 10.4 mmol, 1.20 *eq*) at 70 °C for 12 hrs to give 2-(2-phenethylcyclopropyl)acetonitrile (**6f**, 1.40 g, 7.56 mmol, 86.9% yield), added EtOH (7.00 mL) and H$_2$O (7.00 mL), KOH (1.70 g, 30.2 mmol, 4.00 *eq*), stirred at 100 °C for 16 hrs to give 1-(2-phenethylcyclopropyl)propan-2-one (**6g**, 1.50 g, 6.95 mmol, 92.0% yield). To a solution of 1-(2-phenethylcyclopropyl)propan-2-one (**6g**, 1.00 g, 4.64 mmol, 1.00 *eq*) in DMF (10.0 mL) was added EDCI (1.33 g, 6.95 mmol, 1.50 *eq*), HOBt (751 mg, 5.56 mmol, 1.20 *eq*), DIPEA (1.80 g, 13.9 mmol, 2.42 mL, 3.00 *eq*) and 4-aminocyclohexan-1-ol (773 mg, 5.10 mmol, 1.10 *eq*, HCl), the mixture was stirred at 25 °C for 16 hrs, LC-MS showed **6g** was consumed completely and desired MS (Rt = 0.882 min) was detected, the residue was purified by prep-HPLC (column: Waters Xbridge C18 150*50mm* 10um; mobile phase: [water(10mM NH4HCO3)-ACN];B%: 28%-58%, 11.5min) to give **6** (99.35 mg, 329 umol, 7.11% yield, 100% purity) as a white solid. **LC-MS:** R$_t$ = 0.895 min, m/z = 302.1 (M+H)$^+$. **HPLC:** R$_t$ = 2.803 min, purity: 100 %, under 220 nm. **¹³C NMR:** (400 MHz MeOD) δ 173.58, 142.27, 128.05, 127.84, 125.25, 69.03, 40.16, 35.84, 35.34, 33.40, 30.14, 17.77, 15.15, 10.80. **¹H NMR:** (400 MHz MeOD) δ 7.27 - 7.23 (m, 2H), 7.19- 7.14 (m, 3H), 3.65 - 3.60 (m, 1H), 3.55 - 3.50 (m, 1H), 2.69 (t, *J* = 7.6 Hz, 2H), 2.09 - 2.02 (m, 2H), 1.97 - 1.89 (m, 4H), 1.75- 1.73 (m, 1H), 1.51 - 1.49 (m, 1H), 1.38 - 1.30 (m, 4H), 0.82 - 0.80 (m, 1H), 0.64 - 0.53 (m, 1H), 0.37 - 0.32 (m, 2H).

N-(4-hydroxycyclohexyl)-3-phenethylcyclobutane-1-carboxamide (7).—A mixture of (2-bromoethyl)benzene (**7a,** 10.0 g, 54.0 mmol, 7.30 mL, 1.00 eq) and

triphenylphosphine (14.2 g, 54.0 mmol, 1.00 eq) was stirred at 100 °C for 16 hrs, then cooled to 20 °C to give compound 2-phenethyl-triphenylphosphonium bromide (**7b**, 20.0 g, 44.4 mmol, 82.2% yield, 99.4% purity), to this was then added toluene (47.0 mL), sodium 2-methylbutan-2-olate (1.16 g, 10.5 mmol, 1.50 *eq*), and the mixture stirred at 20 °C for 0.5 hrs under N_2, at which point a solution of ethyl 3-oxocyclobutane-1-carboxylate (1.00 g, 7.03 mmol, 1.00 *eq*) in toluene (10.0 mL) was added dropwise to the mixture and the mixture was stirred at 70 °C for 4 hrs under N_2 then concentrated under reduced pressure to give a residue that was purified by Reverse Phase HPLC to give ethyl 3-(2phenylethylidene)cyclobutane-1-carboxylate (0.30 g, 1.14 mmol, 16.2% yield, 87.7% purity), then added EtOH (24.0 mL), Pd/C (0.24 g, 10.0% purity) under N_2, the suspension was degassed and purged with H_2 for 3 times, the mixture was stirred at 20 °C for 16 hrs under H_2 (15 psi) then filtered through kieselguhr and the filter residue was washed with ethyl acetate (60.0 mL), the layer was concentrated under reduced pressure to give ethyl 3-phenethylcyclobutane-1-carboxylate (**7c**, 1.10 g, 2.46 mmol, 47.1% yield, 51.9% purity). To a solution of ethyl **7c** (1.10 g, 2.46 mmol, 1.00 *eq*) in MeOH (5.00 mL), THF (10.0 mL) and H_2O (5.00 mL) was added LiOH•H_2O (412 mg, 9.83 mmol, 4.00 *eq*), stirred at 20 °C for 2 hrs, the mixture was concentrated under reduced pressure to give a residue, the residue was poured into H_2O (30.0 mL) and extracted with ethyl acetate (30.0mL * 2), the water phase was adjust pH to 3 ~ 4 with 1 N HCl (10.0 mL) and extracted with ethyl acetate (50.0 mL * 3), the combined layers were dried over Ns_2SO_4, filtered and concentrated under reduced pressure to give 3-phenethylcyclobutane-1-carboxylic acid (**7d,** 0.64 g, 1.79 mmol, 72.6% yield, 57.0% purity) as a yellow oil. To a solution of **7d** (0.64 g, 1.79 mmol, 1.00 *eq*) in DMF (5.00 mL) was added HOBt (362 mg, 2.68 mmol, 1.50 *eq*), EDCI (445 mg, 2.32 mmol, 1.30 *eq*), DIPEA (692 mg, 5.36 mmol, 93 μL, 3.00 *eq*) and 4-aminocyclohexan-1-ol (325 mg, 2.14 mmol, 1.20 *eq*, HCl), stirred at 20 °C for 16 hrs. The mixture was purified by prep-HPLC (column: Waters Xbridge C18 150*50mm* 10um; mobile phase: [water (10mM NH4HCO3) -ACN]; B%: 28%-58%, 11.5min) to give **7** (111.58 mg, 370 umol, 20.7% yield, 100% purity) as a white solid. **LCMS**: Rt = 0.813 min, m/z = 302.2 $(M+H)^+$; Rt = 0.883 min, m/z = 302.1 $(M+H)^+$. **HPLC**: purity: 100% under 220nm. **^{1}H NMR**: (400 MHz MeOD) δ 7.25 - 7.21 (m, 2H), 7.15 - 7.13 (m, 3H), 3.59 - 3.49 (m, 2H), 2.82 - 2.80 (m, 1H), 2.53 - 2.50 (m, 2H), 2.18 - 2.16 (m, 3H), 1.92 - 1.67 (m, 8H), 1.32 - 1.27 (m, 4H). **^{13}C NMR**: (400 MHz MeOD) δ 177.895, 176.889, 143.747, 129.521, 129.422, 126.826, 70.621, 39.844, 39.737, 37.306, 35.031, 34.421, 32.781, 32.435, 31.676, 31.198.

2-(3-benzylcyclobutyl)-N-(4-hydroxycyclohexyl)acetamide (8).—To a solution of allylbenzene (**8a**) (20.0 g, 169 mmol, 22.4 mL, 1.00 *eq*), ZINC-COPPER COUPLE (65.5 g, 508 mmol, 3.00 *eq*) in Et_2O (200 mL), dropwise 2,2,2-trichloroacetyl chloride (61.6 g, 338 mmol, 37.8 mL, 2.00 *eq*) and $POCl_3$ (29.2 g, 190 mmol, 17.7 mL, 1.12 *eq*) in Et_2O (100 mL) at 20 °C under N_2 for 2 hrs, then the reaction was stirred at 35°C for 16 hrs, the mixture was filtered through a pad of celite and the filtrate was poured into water (300 mL) and extracted with Et_2O (200 mL * 3), the organic layer was washed with saturated $NaHCO_3$ (200 mL * 2) and brine (200 mL), dried over Na_2SO_4, filtered and concentrated under reduced pressure to give 3-benzyl-2,2-dichlorocyclobutan-1-one (**8b,** 46.2 g). To a solution of ZINC (52.8 g, 807 mmol, 4.00 *eq*) in AcOH (120 mL) was added **8b** (46.2 g, 202 mmol, 1.00 *eq*) in AcOH (120 mL) dropwise at 25 °C for 1 hr,

stirred at 25 °C for 1 hr and then heated at 80 °C for 1 hr, the mixture was filtered and poured into water (200 mL), extracted with EtOAc (200 mL * 3), the organic layer was combined and washed with $NaHCO_3$ (saturated, 150 mL * 2) and brine (200 mL), dried over Na_2SO_4, filtered and concentrated under reduced pressure and was purified by Reverse Phase HPLC (0.1% FA condition) to get 3-benzylcyclobutan-1-one (14.8 g, 78.6 mmol, 38.9% yield, 85.0% purity), to a solution of 3-benzylcyclobutan-1-one (1.00 g, 5.31 mmol, 1.00 eq) in toluene (20 mL) was added methyl 2-(triphenyl-l^5-phosphaneylidene)acetate (2.66 g, 7.96 mmol, 1.50 eq), stirred at 110 °C for 2 hrs, the reaction was concentrated under vacuum to get a residue and triturated with petroleum ether (20 mL) at 25 °C for 10 mins, the product was purified by prep-HPLC (column: Phenomenex luna C18 150 * 40mm * 15 μm; mobile phase: [water (0.225% FA) - ACN]; B%: 47% - 77%, 10 mins) to get methyl 2-(3 benzylcyclobutylidene)acetate (943 mg, 4.34 mmol, 81.8% yield, 99.5% purity). To a solution of methyl 2-(3-benzylcyclobutylidene)acetate (943 mg, 4.34 mmol, 1.00 eq) in MeOH (20 mL) was added Pd/C (0.20 g, 10% purity), the reaction was degassed and back filled with H_2 (15 psi) and stirred at 25 °C for 2 hrs, the residue was filtered through diatomite and the filtrate was concentrated under vacuum to afford methyl 2-(3-benzylcyclobutyl)acetate (**8c**, 947 mg, 4.31 mmol, 99.2% yield, 99.3% purity), to a solution of **8c** (947 mg, 4.31 mmol, 1.00 eq) in THF (10 mL), H_2O (5 mL) and MeOH (5 mL) was added LiOH•H_2O (723 mg, 17.2 mmol, 4.00 eq), the reaction mixture was stirred at 25 °C for 16 hrs, then the reaction mixture was concentrated to get a residue, and was poured into H_2O (15 mL) and extracted with EtOAc (15 mL * 3), the aqueous layer was adjusted pH = 2 ~ 3 and extracted with EtOAc (15 mL * 3), dried over Na_2SO_4, filtered and concentrated under reduced pressure to give 2-(3-benzylcyclobutyl)acetic acid (**8d**, 877 mg, 4.05 mmol, 94.0% yield, 94.4% purity) as a light yellow oil. To a solution of **8d** (300 mg, 1.39 mmol, 1.00 eq) in DMF (5 mL) was added HOBt (225 mg, 1.66 mmol, 1.20 eq), EDCI (399 mg, 2.08 mmol, 1.50 eq) and DIEA (538 mg, 4.16 mmol, 724 μL, 3.00 eq), aminocyclohexan-1-ol (241 mg, 1.53 mmol, 1.10 eq, HCl) was added to the mixture. The reaction mixture was stirred at 25 °C for 16 hrs, the reaction mixture was poured into H_2O (15 mL) and extracted with EtOAc (10 mL * 3), the organic layer was dried over Na_2SO_4, filtered and concentrated under reduced pressure to give a residue and was purified by prep-HPLC (column: Phenomenex luna C18 150 * 40mm * 15 μm; mobile phase: [water (0.225% FA) - ACN]; B%: 23% - 53%, 9 mins) to get **8** (111.58 mg, 366 μmol, 26.3% yield, 98.8% purity) as a white solid. **LCMS**: Rt = 0.794 min, m/z = 302.1 $(M+H)^+$; Rt = 0.787 min, m/z = 302.2 $(M+H)^+$. **HPLC**: Rt = 2.682 min, purity: 98.8% under 220 nm. **^{1}H NMR**: (400 MHz, MeOD) δ 7.24 - 7.20 (m, 2H), 7.14 - 7.12 (m, 3H), 3.60 - 3.51 (m, 2H), 2.74 - 2.63 (m, 3H), 2.30 - 2.28 (m, 2H), 2.20 - 2.18 (m, 2H), 1.94 - 1.84 (m, 6H), 1.45 - 1.42 (m, 1H), 1.32 - 1.24 (m, 4H). **^{13}C NMR**: (400 MHz, MeOD) δ 174.65 - 174.39, 142.47 - 142.21, 129.76 - 129.36, 129.90, 70.57, 44.61 - 44.49, 43.73 - 43.46, 35.63, 34.97, 34.36, 33.24, 31.71, 30.65, 30.18.

N-((1*r*,4*r*)-4-hydroxycyclohexyl)-3-phenethylcyclopentane-1-carboxamide (9).—

A mixture of dimethyl cyclopentane-1,3-dicarboxylate (**9a**, 2.00 g, 10.7 mmol, 1.00 eq) and NaOH (429 mg, 10.7 mmol, 1.00 eq) in MeOH (10.0 mL) was stirred for 12 hrs at 25 °C, filtered and concentrated under reduced pressure to give a residue, purified by column chromatography to get 3-(methoxycarbonyl)cyclopentane-1-carboxylic acid (**9b**,

1.20 g, 6.97 mmol, 64.8% yield) as a light yellow oil. To a mixture of **9b** (1.10 g, 6.39 mmol, 1.00 eq) in THF (10.0 mL) was added BH_3-Me_2S (10.0 M, 703 uL, 1.10 eq) at −78 °C, stirred for 0.5 hr, then warmed to 25 °C and stirred for 12 hrs to obtain methyl 3-(hydroxymethyl)cyclopentane-1-carboxylate (**9c**, 780 g, 4.93 mmol, 77.1% yield) was obtained as a yellow oil. To a mixture of **9c** (780 mg, 4.93 mmol, 1.00 eq) in DCM (10.0 mL) was added Dess-Martin (2.72 g, 6.41 mmol, 1.30 eq) at 25 °C and was stirred for 2 hrs, dried over Na_2SO_4, filtered and concentrated under reduced pressure to give a residue and was purified by column chromatography to obtain methyl 3-formylcyclopentane-1-carboxylate (9d, 283 mg, 1.81 mmol, 36.7% yield) was obtained as a light yellow oil. To a solution of benzyltriphenylphosphonium bromide (**9e**, 903 mg, 2.08 mmol, 1.15 eq) in THF (10.0 mL) was added t-BuOK (329 mg, 2.94 mmol, 1.62 eq) at −20 °C under N_2, stirred for 1 hr at −20 °C and then added **9d** (183 mg, 1.81 mmol, 1.00 eq) at −20 °C and stirred another 1 hr, filtered and concentrated under reduced pressure to give a residue and was purified by column chromatography to get methyl (*E*)-3-styrylcyclopentane-1-carboxylate (124 mg, 538 umol, 29.7% yield) was obtained as a light yellow oil. To a solution of (*E*)-3-styrylcyclopentane-1-carboxylate (124 mg, 538 umol, 1.00 eq) in MeOH (10.0 mL) was added Pd/C (120 mg, 10% purity) at 25 °C under H_2 (15 Psi), stirred for 2 hrs at 25 °C to get methyl 3-phenethylcyclopentane-1-carboxylate (**9f**, 100 mg, 430 umol, 79.9% yield) was obtained as a light yellow oil. To a mixture of **9f** (85.0 mg, 365 umol, 1.00 eq) in MeOH (5.00 mL), THF (5.00 mL) and H_2O (2.00 mL) was added LiOH·H_2O (30.7 mg, 731 umol, 2.00 eq) at 25 °C, the mixture was heated to 70 °C and stirred for 2 hrs to get 3-phenethylcyclopentane-1-carboxylic acid (**9g**, 79.0 mg, 361 umol, 98.9% yield) as a light yellow oil. To a mixture of **9g** (79.0 mg, 361 umol, 1.00 eq) and (1*r*,4*r*)-4-aminocyclohexan-1-ol (65.8 mg, 434 umol, 1.20 eq) in THF (10.0 mL) was added HATU (206 mg, 542 umol, 1.50 eq) and Et_3N (727 mg, 7.18 mmol, 1.00 mL) at 25 °C and stirred for 12 hrs. The reaction mixture was concentrated under reduced pressure to give a residue. The reside was purified by prep-HPLC (neutral condition,column: Waters Xbridge 150*25mm*5um;mobile phase: [water(NH_4HCO_3)-ACN];B%: 43%−73%, 10min). **9** (8.24 mg, 25.2 umol, 6.97% yield, 96.5% purity) was obtained as a white solid. **LCMS**: RT = 0.933 min, m/z = 316.2 $(M+H)^+$. **HPLC**: RT = 2.130 mins, purity: 96.5% purity, under 220 nm. ^{1}**H NMR**: (400 MHz, DMSO-d_6) δ 7.52 (d, *J* = 7.6, 1H), 7.27-7.23 (m, 2H), 7.18-7.15 (m, 3H), 4.52 (d, *J* = 4.0, 1H), 3.43-3.41 (m, 1H), 2.57-2.53 (m, 2H), 1.87 - 1.57 (m, 12H), 1.18-1.06 (m, 7H).

N-((1*r*,4*r*)-4-hydroxycyclohexyl)-3-(3-phenylpropyl)cyclopentane-1-carboxamide (10)—To a solution of triphenyl(3-phenylpropyl)phosphonium bromide (**10b**, 1.79 g, 3.87 mmol, 1.10 *eq*) in toluene (10.00 mL) was added t-BuOK (473 mg, 4.22 mmol, 1.20 *eq*), the mixture was stirred at 70 °C for 1 hr. Then methyl 3-oxocyclopentane-1-carboxylate (**10a**, 500 mg, 3.52 mmol, 1.00 *eq*) in toluene (2.00 mL) was added to the mixture and stirred at 70 °C for 16 hrs to give methyl 3-(3-phenylpropylidene)cyclopentane-1-carboxylate (0.100 g, 388 umol, 11.0% yield, 94.8% purity) as a colorless oil, MeOH (10.0 mL), Pd/C (0.10 g, 10% purity) were added at 25 °C, degassed with N_2 for 3 times. The resulting mixture was stirred at 25 °C under H_2 (15 Psi) for 4 hrs, the mixture was filtered through celite and the filtrate was concentrated under vacuum to give methyl 3-(3-phenylpropyl)cyclopentane-1-

carboxylate (**10c**, 90.0 mg, 365 umol, 94.1% yield) was obtained as a colorless oil. A solution of **10c** (90.0 mg, 365 umol, 1.00 *eq*) and LiOH·H$_2$O (30.6 mg, 730 umol, 2.00 *eq*) in MeOH (5.00 mL) and H$_2$O (2.00 mL) was stirred at 70 °C for 3 hrs to obtain 3-(3-phenylpropyl)cyclopentane-1-carboxylic acid (**10d**, 90.0 mg, crude) was obtained as a yellow oil. A mixture of **10d** (90.0 mg, 387 umol, 1.00 *eq*), (1*r*,4*r*)-4-aminocyclohexan-1-ol (49.0 mg, 426 umol, 1.10 *eq*), HATU (294 mg, 774 umol, 2.00 *eq*) and Et$_3$N (117 mg, 1.16 mmol, 161 uL, 3.00 *eq*) in THF (2.00 mL) was stirred at 25 °C for 16 hrs, the mixture was concentrated to give the residue, then purified by column: Phenomenex Gemini-NX C18 75*30mm*3um;mobile phase: [water(0.225%FA)-ACN]; B%: 42%-72%,7min. **11** (23.38 mg, 68.1 umol, 17.6% yield, 96.1% purity) was obtained as an off-white solid. **LCMS**: RT = 0.859 min, m/z = 330.3 (M+H)$^+$. **HPLC**: RT = 2.548 mins, purity: 96.1%, under 220 nm. **^{1}H NMR**: (400 MHz, DMSO-d_6)δ 7.47 (d, *J* = 8.0, 1H), 7.28-7.24 (m, 2H), 7.18-7.15 (m, 3H), 4.49 (d, *J* = 4.0, 1H), 3.43-3.37 (m, 1H), 2.58-2.53 (m, 3H), 1.78 - 1.77 (m, 1H), 1.76 - 1.70 (m, 3H), 1.68 - 1.66 (m, 5H), 1.64-1.54 (m, 3H), 1.32-1.29 (m, 3H), 1.18-1.13 (m, 6H).

N-((1*r*,4*r*)-4-hydroxycyclohexyl)-3-phenethylcyclohexane-1-carboxamide (11).
—To a mixture of 3-(methoxycarbonyl)cyclohexane-1-carboxylic acid (**11a**, 2.00 g, 10.7 mmol, 1.00 eq) in THF (10.0 mL) was added BH$_3$-Me$_2$S (10.0 M, 1.18 mL, 1.10 eq) at −78 °C and stirred for 0.5 hr at −78 °C, then warmed to 25 °C and stirred for 12 hrs to obtain methyl 3-(hydroxymethyl)cyclohexane-1-carboxylate (**11b**, 1.79 g, 10.4 mmol, 96.7% yield) was obtained as a light yellow oil. To a mixture of **11b** (1.79 g, 10.4 mmol, 1.00 eq) and Et$_3$N (6.31 g, 62.3 mmol, 6.00 eq) in DMSO (20.0 mL) was added pyridine;sulfur trioxide (4.96 g, 31.2 mmol, 3.00 eq) at 25 °C and stirred for 12 hrs, dried over Na$_2$SO$_4$, filtered and concentrated under reduced pressure to give a residue. The residue was purified by column chromatography to get methyl 3-formylcyclohexane-1-carboxylate (**11c**, 710 mg, 4.17 mmol, 40.1% yield) was obtained as a yellow oil. To a solution of benzyltriphenylphosphonium bromide (1.17 g, 2.70 mmol, 1.15 eq) in THF (10.0 mL) was added t-BuOK (427 mg, 3.81 mmol, 1.62 eq) at −20 °C under N$_2$, was stirred for 1 hr at −20 °C and then added **11c** (400 mg, 2.35 mmol, 1.00 eq) at −20 °C and stirred another 1 hr. The product was dried over Na$_2$SO$_4$, filtered and concentrated under reduced pressure to give a residue. The residue was purified by column chromatography to get intermediate methyl (*E*)-3-styrylcyclohexane-1-carboxylate (280 mg, 1.15 mmol, 48.7% yield) was obtained as a light yellow oil, then added MeOH (10.0 mL) was added Pd/C (230 mg, 10% purity) at 25 °C under H$_2$ (15 Psi), stirred for 2 hrs to get methyl 3-phenethylcyclohexane-1-carboxylate (**11d**, 230 mg, 933 umol, 87.7% yield) was obtained as a colourless oil. To a mixture of **11d** (165 mg, 669 umol, 1.00 eq) in MeOH (5.00 mL), THF (5.00 mL) and H$_2$O (2.00 mL) was added LiOH·H$_2$O (56.2 mg, 1.34 umol, 2.00 eq) at 25 °C then heated to 70 °C and stirred for 2 hrs to get 3-phenethylcyclohexane-1-carboxylic acid (**11e**, 150 mg, 645 umol, 96.4% yield) was obtained as a light yellow oil. To a mixture of **11e** (150 mg, 645 umol, 1.00 eq) and (1*r*,4*r*)-4-aminocyclohexan-1-ol (117 mg, 774 umol, 1.20 eq) in THF (10.0 mL) was added HATU (368 mg, 968 umol, 1.50 eq) and Et$_3$N (1.45 g, 14.3 mmol, 2.00 mL) at 25 °C, stirred at 25 °C for 12 hrs. The reaction mixture was concentrated under reduced pressure to give a residue and was purified by prep-HPLC (neutral condition, column: Waters Xbridge 150*25mm*5um;mobile phase: [water(NH$_4$HCO$_3$)-ACN];B%: 40%−70%,10min). **11** (8.15 mg, 24.3 umol, 3.78% yield, 98.6% purity) was obtained as a white solid. **LCMS**: RT =

0.930 min, m/z = 330.2 (M+H)$^+$. **HPLC**: RT = 2.218 mins, purity: 98.6%, under 220 nm. **^{1}H NMR**: (400 MHz, DMSO-d_6)δ 7.46 (d, J = 8.0, 1H), 7.27-7.24 (m, 2H), 7.19-7.14 (m, 3H), 4.49 (s, 1H), 3.42-3.38 (m, 1H), 2.59-2.55 (m, 2H), 2.04-1.98 (m, 1H), 1.79 - 1.69 (m, 8H), 1.58-1.40 (m, 4H), 1.24-1.11 (m, 6H), 1.09-0.96 (m, 1H), 0.90-0.77 (m, 1H).

N-((1*r*,4*r*)-4-hydroxycyclohexyl)-4-phenethylcyclohexane-1-carboxamide (12).

—A mixture of benzyltriphenylphosphonium bromide (1.47 g, 3.39 mmol, 1.15 eq) and t-BuOK (535 mg, 4.77 mmol, 1.62 eq) in THF (10.0 mL) at −20 °C under N$_2$ and was stirred for 1 hr, then added 4-formylcyclohexane-1-carboxylic acid (**12a**, 500 mg, 2.94 mmol, 1.00 eq) at −20 °C and stirred another 1 hr, dried over Na$_2$SO$_4$, filtered and concentrated under reduced pressure to give a residue and was purified by column chromatography to obtain intermediate methyl (*E*)-4-styrylcyclohexane-1-carboxylate (130 mg, 530 umol, 18.1% yield, 99.7% purity) was obtained as an off-white solid, then added MeOH (10.0 mL), Pd/C (120 mg, 10% purity) at 25 °C under H$_2$ (15 Psi), stirred for 2 hrs to get methyl 4-phenethylcyclohexane-1-carboxylate (**12b**, 120 mg, 487 umol, 91.5% yield) was obtained as a light yellow oil. To a mixture of **12b** (120 mg, 487 umol, 1.00 eq) in MeOH (5.00 mL), THF (5.00 mL) and H$_2$O (2.00 mL) was added LiOH·H$_2$O (40.9 mg, 974 umol, 2.00 eq) at 25 °C, then heated to 70 °C and stirred for 2 hrs to get 4-phenethylcyclohexane-1-carboxylic acid (**12c**, 110 mg, 473 umol, 97.2% yield) was obtained as a light yellow oil, then added (1*r*,4*r*)-4-aminocyclohexan-1-ol (65.4 mg, 568 umol, 1.20 eq) in THF (10.0 mL) was added HATU (270 mg, 710 umol, 1.50 eq) and Et$_3$N (143 mg, 1.42 mmol, 3.00 eq) at 25 °C and stirred for 12 hrs. The reaction mixture was concentrated under reduced pressure to give a residue and was purified by prep-HPLC (neutral condition, column: Waters Xbridge 150*25mm*5um;mobile phase: [water(10mM NH$_4$HCO$_3$)-ACN];B%: 40%-70%,10min). **12** (9.82 mg, 29.3 umol, 6.21% yield, 98.6% purity) was obtained as a white solid. **LCMS**: RT = 0.859 min, m/z = 330.3 (M+H)$^+$. **HPLC**: RT = 2.236 mins, purity: 98.6%, under 220 nm. **^{1}H NMR**: (400 MHz, DMSO-d_6)δ 7.45 (d, J = 8.0, 1H), 7.27-7.24 (m, 2H), 7.18-7.15 (m, 3H), 4.48 (d, J = 4.0, 1H), 3.46-3.36 (m, 2H), 2.59-2.55 (m, 2H), 2.03-1.96 (m, 1H), 1.80 - 1.76 (m, 4H), 1.69-1.64 (m, 4H), 1.45-1.43 (m, 2H), 1.35-1.25 (m, 2H), 1.25-1.13 (m, 5H), 0.91-0.87 (m, 2H).

4-benzyl-*N*-((1*r*,4*r*)-4-hydroxycyclohexyl)cyclohexane-1-carboxamide (13).—A

mixture of methyl 4-(4,4,5,5-tetramethyl-1,3,2-dioxaborolan-2-yl)cyclohex-3-ene-1-carboxylate (**13a**, 500 mg, 1.88 mmol, 1.15 eq) and (bromomethyl)benzene (385 mg, 2.25 mmol, 1.20 eq) in dioxane (10.0 mL) and H$_2$O (2.00 mL) was added Pd(dppf)Cl$_2$ (274 mg, 375 umol, 0.20 eq) and K$_2$CO$_3$ (778 mg, 5.64 mmol, 3.00 eq) at 25 °C under N$_2$. The mixture was heated to 100 °C and stirred for 2 hrs to get intermediate methyl 4-benzylcyclohex-3-ene-1-carboxylate(300 mg, 1.30 mmol, 69.3% yield) was obtained as a light yellow oil. To a solution of the intermediate (300 mg, 1.30 mmol, 1.00 eq) in MeOH (10.0 mL) was added Pd/C (300 mg, 10% purity) at 25 °C under H$_2$ (15 Psi) and was stirred for 2 hrs at 25 °C to obtain methyl 4-benzylcyclohexane-1-carboxylate (**13b,** 300 mg, 1.29 mmol, 99.1% yield) was obtained as a light yellow oil. To a mixture of **13b** (300 mg, 1.29 mmol, 1.00 eq) in MeOH (5.00 mL), THF (5.00 mL) and H$_2$O (2.00 mL) was added LiOH·H$_2$O (108 mg, 2.58 mmol, 2.00 eq) at 25 °C and then heated to 70 °C and stirred for 2 hrs to get 4-benzylcyclohexane-1-carboxylic acid (**13c**, 280 mg, 1.28 mmol, 99.3% yield)

was obtained as a light yellow oil. To a mixture of **13c** (280 mg, 1.28 mmol, 1.00 eq) and (1*r*,4*r*)-4-aminocyclohexan-1-ol (147 mg, 1.28 mmol, 1.00 eq) in THF (5.00 mL) was added HATU (731 mg, 1.92 mmol, 1.50 eq) and Et$_3$N (389 mg, 3.85 mmol, 3.00 eq) at 25 °C and stirred for 12 hrs. The reaction mixture was concentrated under reduced pressure to give a residue. The reside was purified by prep-HPLC (neutral condition, column: Waters Xbridge 150*25mm*5um;mobile phase: [water(10mM NH$_4$HCO$_3$)-ACN];B%: 37%-67%,10min). **13** (58.93 mg, 185 umol, 14.4% yield, 99.0% purity) was obtained as a white solid. **LCMS**: RT = 0.823 min, m/z = 316.3 (M+H)$^+$. **HPLC**: RT = 2.097 mins, purity: 99.0%, under 220 nm. **^{1}H NMR**: (400 MHz, CDCl$_3$-*d$_1$*)δ 7.21-7.17 (m, 2H), 7.11-7.05 (m, 3H), 5.24 (d, *J* = 7.6, 1H), 3.72-3.68 (m, 1H), 3.54-3.51 (m, 1H), 2.52 (d, *J* = 7.6, 2H), 2.15 - 2.13 (m, 1H), 1.93-1.91 (m, 4H), 1.84-1.66 (m, 4H), 1.46-1.36 (m, 7H), 1.12-1.09 (m, 2H).

2-((benzylthio)methyl)-N-((1r,4r)-4-hydroxycyclohexyl)cyclopropane-1-carboxamide (14, 14A and 14B).—Phenylmethanethiol (**14a**,

25.2 g, 202 mmol, 23.7 mL, 1.00 *eq*) was added to a solution of EtONa (13.8 g, 202 mmol, 1.00 *eq*) in EtOH (100 mL), KI (1.68 g, 10.1 mmol, 0.05 *eq*) and 2-chloro-1,1-dimethoxyethane (30.3 g 243 mmol, 27.8 mL, 1.20 *eq*), the mixture was stirred at 80 °C for 12 hrs, the reaction mixture was filtered, concentrated under reduced pressure and purified by flash silica gel chromatography to obtain benzyl(2,2-dimethoxyethyl)sulfane (38.0 g, 179 mmol, 88.2% yield), added H$_2$SO$_4$ (17.9 g 179 mmol, 9.74 mL, 98.0% purity, 1.00 *eq*) and stirred at 60 °C for 12 hrs to obtain 2-(benzylthio)acetaldehyde (**14b**, 27.0 g). *Tert*-butyl 2-(triphenyl-λ5-phosphaneylidene)acetate (64.7 g, 172 mmol, 1.30 *eq*) was added into a solution of **14b** (22.0 g, 132 mmol, 1.00 *eq*) in THF (220 mL), stirred at 20 °C for 12 hrs to obtain *tert*-butyl (*E*)-4-(benzylthio)but-2-enoate (**14c**, 31.3 g). To a solution of NaH (3.87 g, 96.6 mmol, 60.0% purity, 1.20 *eq*) in DMSO (100 mL) was added dimethylmethanesulfinic iodide (21.2 g 96.6 mmol, 1.20 *eq*) and the mixture was stirred at 20 °C for 0.5 hr, then added a solution of **14c** (21.3 g, 80.5 mmol, 1.00 *eq*) and stirred at 20 °C for 1 hr to obtain *tert*-butyl 2-((benzylthio)methyl)cyclopropane-1-carboxylate (**14d,** 4.10 g 14.7 mmol, 18.2% yield). To a solution of **14d** (4.10 g, 14.7 mmol, 1.00 *eq*) in DCM (20.0 mL) was added TFA (36.1 g, 316 mmol, 23.4 mL, 21.5 *eq*), the mixture was stirred at 25 °C for 16 hrs to obtain 2-((benzylthio)methyl)cyclopropane-1-carboxylic acid (**14e,** 2.30 g). To a solution of **14e** (2.30 g, 10.3 mmol, 1.00 *eq*) in DMF (20.0 mL) was added EDCI (2.98 g, 15.5 mmol, 1.50 *eq*) , HOBt (1.68 g, 12.4 mmol, 1.20 *eq*) and DIEA (2.68 g, 20.7 mmol, 3.61 mL, 2.00 *eq*). Then (1*r*,4*r*)-4-aminocyclohexan-1-ol (1.73 g, 11.3 mmol, 1.10 *eq*) was added to the mixture and stirred at 25 °C for 2 hrs. The reaction mixture was poured into water (90.0 mL), stirred at 25 °C for 1 hr, filtered and the filtrate was evaporated under vacuum, the product was triturated with Ethyl acetate (30.0 mL) at 70 °C for 30 mins, then cooled to 25 °C, filtered and the filtrate was concentrated under vacuum, the residue was purified by prep-HPLC (column: Phenomenex luna C18 250*50mm*10 um; mobile phase: [water(0.1%TFA)-ACN]; B%: 20%−50%,20min). To get the individual enantiomers **14A** and **14B**, the product was purified by prep-SFC (column: DAICEL CHIRALPAK AD-H (250mm*30mm,5um); mobile phase: [0.1%NH3H2O ETOH]; B%: 35%−35%,2.7 min;240 minmin). The product was purified by (column: Phenomenex Gemini-NX C18 75*30mm*3um; mobile phase: [water (0.05% ammonia hydroxide v/v)-ACN]; B%: 15%−45%,7min) and (column: Phenomenex Gemini-

NX C18 75*30mm*3um;mobile phase: [water(0.225%FA)-ACN]; B%: 30%−60%, 2min). **14A** (1.37 g, 4.22 mmol, 40.7% yield, 98.4% purity) was obtained as an off-white solid, **14B** (1.18 g, 3.59 mmol, 34.7% yield, 97.3% purity) was obtained as an off-white solid. **LCMS: 14A:** RT = 0.816 min, m/z = 320.2 (M+H)[+]; **14B:** : RT = 0.645 min, m/z = 319.9 (M+H)[+]. **HPLC: 14A:** RT = 1.887 mins, purity: 98.4%, under 220 nm. **14B:** RT = 1.880 mins, purity: 97.3%, under 220 nm. **^{1}H NMR: 14A:** (400 MHz MeOD) δ 7.33 - 7.21 (m, 5H), 3.76 (s, 2H), 3.60-3.57 (m, 1H), 3.52 - 3.50 (m, 1H), 2.44 - 2.40 (m, 2H), 1.94 - 1.89 (m, 4H), 1.42 - 1.40 (m, 2H), 1.33 - 1.29 (m, 4H), 1.08 (td, J = 4.4, 8.8 Hz, 1H), 0.69 (ddd, J = 4.2, 6.0, 8.4 Hz, 1H); **14B:** (400 MHz MeOD) δ 7.32 - 7.28 (m, 5H), 3.76 (s, 2H), 3.61-3.58 (m, 1H), 3.52 - 3.50 (m, 1H), 2.44 - 2.40 (m, 2H), 1.94 - 1.89 (m, 4H), 1.43 - 1.41 (m, 2H), 1.33 - 1.28 (m, 4H), 1.08 (td, J = 4.4, 8.8 Hz, 1H), 0.69 (ddd, J = 4.2, 6.0, 8.4 Hz, 1H).

X-ray diffraction studies of 14A and 14B.

X-ray powder diffraction (XRPD) studies were performed with a Panalytical X'Pert[3] Powder XRPD on a Si zero-background holder. The 2θ position was calibrated against a Panalytical Si reference standard disc. The parameters used are shown in Table S2.

TGA/DSCThermogravimetric analysis (TGA) data were collected using a TA Discovery 550 TGA from TA Instrument. **Differential scanning calorimetry (DSC)** was performed using a TA 2500 DSC from TA Instrument. DSC was calibrated with Indium reference standard and the TGA was calibrated using nickel reference standard. Detailed parameters used are shown in Table S3.

Polarized Light Microscopy crystal images were captured on Nikon DS-Fi2 upright microscope at room temperature.

Single Crystal Data Collection

The X-ray intensity data were measured on a Bruker D8 VENTURE (IµS microfocus X-ray source, Cu Kα, λ =1.54178Å, PHOTON CMOS detector) diffractometer. The strategy was created and optimized with the Bruker Apex3 software, and the frames were integrated with the Bruker SAINT software package. Data were corrected for absorption effects using the Multi-Scan method (SADABS-2016/2). The structure was solved with the ShelXT structure solution program using Intrinsic Phasing and refined with ShelXL (Version 2014/7) refinement package using full-matrix least-squares on F[2] contained in the SHELX software suite.[24,25]

Single Crystal Growth Experiments

Slow Evaporation—HPLC vials with saturated solutions of **14A** and **14B** were capped with perforated caps. Vials were left at RT to allow slow evaporation of the solvents. A total of 20 experiments were prepared, 4 of which are represented in the table below. The remaining 16 samples were moved to slow cooling due to limited observed solubility. Summary of slow evaporation experiments are shown in Table S4.

Layer Diffusion was performed in HPLC vials with saturated solutions of **14A** and **14B**. Anti-solvent was layered onto the saturated solutions slowly and the vial capped. Vials

were left at room temperature to allow the two solvents to diffuse into one another. A total of 20 experiments were performed with results shown below. Summary of layer diffusion experiments are shown in Table S5.

Slow Cooling—Saturated solutions of **14A** and **14B** were prepared by slurrying at 35-60 ^{0}C in HPLC vials. Suspensions were filtered using a PTFE membrane (pore size 0.20 μm). Filtrates were slowly cooled to 5ºC at a rate of 0.1ºC/min. A total of 15 experiments were performed; results are shown in Table S1.

Dose-response of mitofusin agonist fusogenicity, measured using a mitochondrial elongation assay (aspect ratio) was performed in Mfn1- or Mfn2-deficient MEFs cultured at 37°C, 5% CO2-95% air, cells were seeded on day 1 in 6 well plates at a density of $2x10^4$ cells per well and compounds added at 9 concentrations (0.5nM-10uM dissolved in DMSO) overnight. Mitochondria were then stained with MitoTracker Orange (200 nM; M7510; Invitrogen, Carls-bad, CA, USA), nuclei were stained with Hoechst (10 μg/ml; Invitrogen, Thermo Fisher Scientific Cat: # H3570). Images were acquired at room temperature on a Nikon Ti Confocal microscope using a 60 X 1.3 NA oil- immersion objective in Krebs-Henseleit buffer (138 NaCl, 3.7 nM KCL, 1.2 nM KH2PO4, 15 nM Glucose, 20 nM HEPES pH: 7.2-7.5, and 1 mM CaCl2). Laser excitation was 549 nm with emission at 590 nm for MitoTracker Orange and excitation at 306 nm with emission at 405 nm for Hoechst. Images were analyzed using ImageJ and fusogenicity quantified as mitochondrial aspect ratio (length/width), and were indexed to the maximal response elicited by 1 and response curves interpolated using the sigmoidal model using Prism 8 software. EC50 values are reported as mean with 95% confidence limits for at least 3 independent experiments ([16]).

<u>**Functional evaluation of mitofusin agonist effect on mitochondrial depolarization.:**</u> Cultured Mfn2 KO or Mfn1 KO MEFs treated with either DMSO, **1**, **5A** or **5B** (1 μM) for 48 hours, then were stained with Tetramethylrhodamine ethyl ester (TMRE, 200 nM, Invitrogen Thermo Fisher Scientific Cat:# T-669) , MitoTracker Green (200 nM; Invitrogen, Thermo Fisher Scientific Cat:# M7514) and Hoechst (10 ug/ml; Invitro-gen, Thermo Fisher Scientific Cat:# H3570) for 30 min at 37°C in 5% CO2-95% air, washed twice in PBS. Images were acquired at room temperature on a Nikon Ti Confocal microscope using either 60 X 1.3 NA oil- immersion ob-jective, in Krebs-Henseleit buffer (138 NaCl, 3.7 nM KCL, 1.2 nM KH2PO4, 15 nM Glucose, 20 nM HEPES pH: 7.2-7.5, and 1mM CaCl2): laser excitation was 488 nm with emission at 510 nm for MitoTracker Green, 549 nm with emission at 590 nm for TMRE, and 306 nm with emission 405 nm for Hoechst. Mitochondrial depolarization was reported as % number of green mitochondria/number of yellow+green mitochondria using Image J. ([16]).

FRET studies of MFN2 conformation were performed as previously described ([15, 16]). Briefly, the MFN2 FRET protein engineered with amino terminal mCerulean and carboxy terminal mVenus reporters ([14]) was expressed with an adenoviral vector in mitofusin null (MFN1/MFN2 knockout) MEFs cultured in UV transparent 96 well plates. 48 hours thereafter 1 μM of each test compound or vehicle (DMSO) was added for 4 hours. Fluorescence signals were acquired on a Tecan Safire II multi-mode plate reader: FRET-excitation 433/8 nm, emission 528/8 nm; Cerulean-excitation 433/8 nm, emission 475/8 nm.

Mitofusin agonist pharmacodynamic effects on sciatic nerve motility were measured using time-lapse imaging (1 frame every 5 s) for 121 frames (10 min, sciatic nerve) at 37°C on a Nikon A1Rsi Confocal Microscope using a 40x oil objective as described. Sciatic nerve axon mitochondria were labeled with TMRE. Kymographs and quantitative data were generated using an Image-J plug-in ([17]).

In vitro **pharmacokinetic analyses** of mitofusin agonists were performed in duplicate using standard methods by WuXi Apptec Co. Ltd. (Shanghai, China). **Plasma protein binding** was measured by equilibrium dialysis; % bound = (1-[free compound in dialysate]/[total compound in retentate]) X 100. Plasma stability of 2 μM compounds in clarified freeze-thawed plasma was assessed by LC-MS/MS of supernatants after protein precipitation; 120 min data are reported for studies including 0, 10, 30, 60, and 120 min. **Liver Microsome stability** of 1 μM compounds in liver microsomes (0.5 mg/ml) after 0, 5, 10, 20, 30, 60 min. incubation was assessed by LC/MS/MS of reaction extracts. **Passive artificial blood brain barrier membrane permeability assay (PAMPA-BBB)** were performed using 150 μL of 10 μM compounds (5% DMSO) added to PVDF membranes pre-coated with 5 μL of 1% brain polar lipid extract (Porcine)/dodecane mixture and incubated for 4h at room temperature with shaking at 300 rpm. Donor and acceptor samples were analyzed by LC-MS/MS.

In vivo **pharmacokinetic analyses** were performed in triplicate at WuXi Apptec Co. Ltd. (Shanghai, China) or Frontage Laboratories, Inc (Exton PA, USA). Except where specifically noted, compounds were administered orally to mice fasted overnight with food returned 4 hours post-dosing. Compound **2** and **5B** (5mg/mL) were dissolved in 30% SBE-β-CD and administered by oral gavage (50 mg/kg) to 7-9 week male CD-1 mice, plasma was collected and brains were prepared by homogenizing with 4 volumes (w:v) of homogenizing solution (MeOH/15 mM PBS (1:2, v:v)) followed by further diluting in blank matrix to obtain dilution factor of 40 and 10. A 40 uL aliquot of the study sample was quenched with 800 μL of IS1 (6 in 1 internal standard in ACN (Labetalol & tolbutamide & Verapamil & dexamethasone & glyburide & Celecoxib 100 ng/mL for each)) respectivelly, and then the mixture was vortex-mixed well (at least 15 s) and centrifuged for 15 min at 12000 × g, 4 °C, an aliquot of 60 μL supernatant was transferred to the 96-well plate and centrifuged for 5 min at 3220 × g, 4 °C, then the supernatant was directly injected for HPLC analysis. Compound **5** enantiomeric mixture was dissolved in 10%DMSO/90%(30%HP-b-CD) and administered intravenously (10 mg/kg) or **5B** (5mg/mL) was dissolved in 10%DMSO/90%(30%HP-b-CD) and administered by oral gavage (50 mg/kg) to 7-9 week male CD-1 mice. Plasma was collected, brain, nerve and spinal cord samples were homogenized in water with 4, 8, and 4 dilution factors, respectively. Plasma, spinal cord, and nerve homogenates were further diluted in control mouse plasma to achieve a total dilution factor of 10, 20, and 40, respectively. For mouse study samples, 30 μL of each sample was added to separate wells of the 96-well plate and 30 μL of diluent (ACN:H$_2$O, 50:50) was added to each sample. To all samples, 200 μL of internal standard (200 ng/mL warfarin) solution in ACN was added. The plate was vortexed vigorously for 10 minutes and then centrifuged for 10 minutes at 4000 rpm (Sorvall Legend X1R centrifuge, Thermo Scientific) at 15°C. Supernatants were further diluted 1:1 in H$_2$O prior to HPLC analysis. Time-concentration

curves were generated using non-compartmental approaches and Phoenix WinNonlin 6.3 software. Data are presented as mean±SEM from 3 mice for each condition.

Measuring effects of 2 and 5 on neuromuscular dysfunction in murine ALS.: ALS (SOD1 G93A) mice ([24]) were randomly assigned to oral treatment with vehicle (10% Me2SO/90% (30% 2-hydroxypropyl)-β-cyclodextrin (HP-BCD; Sigma, Cat :#332607) or **5** (60mg/kg twice daily) from age 60 through 140 days. Disease severity was assessed by investigators blind to treatment status using an integrated multi-test scoring system ([25]) as follows:

Ledge test: Score 0 = effectively use its hind legs while walking along the ledge of the cage; Score 1= loses its footing some times while walking along the ledge, but appears coordinated; Score 2= it does not effectively use its hind legs; Score 3= refuses to move along the ledge or falls off from the ledge while walking;

Hindlimb clasping: Score 0 = hindlimbs completely splayed outward while being lifted by grasped its tail; Score 1= one hindlimb is partially collapsed toward the abdomen; Score 2= both hindlimbs are partially collapsed toward the abdomen; Score 3= hindlimbs are entirely touching the abdomen;

Gait: Score 0 = it appears normal gait when the mice is allowed to walk; Score 1= it is tremor or appears to limp while walking; Score 2= feet point away from the body while waking; Score 3= it has difficulty moving forward;

Kyphosis: Score 0 = it is able to straighten its spine while walking, no kyphosis is observed; Score 1= it shows mild kyphosis but is able to straighten its spine; Score 2= it is unable to straighten its spine but mild kyphosis; Score 3= severe kyphosis while walking and sitting.

The aggregate dysfunction score as reported is the sum of all four individual test scores.

Lipinski's rule and Central Nervous System Multiparameter Optimization calculation.: Lipinski's rule related compounds properties were calculated using DruLiTo software. Compounds chemical properties were obtained using ACD/Laboratories, version 12.1, for ClogD at pH 7.4, pKa. For calculation of TPSA and ClogP were obtained using Chemdraw 19.1. The CNS MPO scores were calculated as described. ([29])

PAINS Analysis.: All reported compounds were screened for PAINS through FAF-Drugs4 website tool (https://mobyle.rpbs.univ-paris-diderot.fr/cgi-bin/portal.py#welcome) and none were identified as pan assay interference compounds.

Animals.: ALS B6.SOD1-G93A mice ([24]) were purchased from The Jackson Laboratory (Stock No: 004435). Mouse procedures were approved by the Institutional Animal Care and Use Committee of Washington University in St. Louis Protocol ID: 19-0910, by IACUC-SH for the WuXi Corporate Committee for Animal Research Ethics, by Confluence Discovery Technologies Animal Care and Use Committee, and by Frontage Labs Animal Care and Use Committee.

Supplementary Material

Refer to Web version on PubMed Central for supplementary material.

Funding:

Abbreviations

ACN	acetonitrile
ALS	Amyotrophic Lateral Sclerosis
CDI	1,1'-carbonyldiimidazole
CMT2A	Charcot-Marie-Tooth Disease type 2A
DCC	N,N'-dicyclohexylcarbodiimide
DCM	dichloromethane
DEAD	Diethyl azodicarboxylate
DIPEA	N,N-Diisopropylethylamine
DMF	dimethylformamide
DMSO	dimethyl sulfoxide
EDCI	N-Ethyl-N′-(3-dimethylaminopropyl)carbodiimide hydrochloride
EtOAc	ethyl acetate
EtOH	ethanol
FRET	förster resonance energy transfer
HP-b-CD	2-Hydroxyproryl-ß-cyclodextrin
HPLC	high performance liquid chromatography
HRMS	high resolution mass spectrometry
PA	isopropyl alcohol
IMIBK	4-methyl-2-pentanone
IPAc	isopropyls acetate
LC-MS	liquid chromatography tandem mass spectrometry
MEFs	Mouse Embryonic Fibroblasts

MEK	methyl ethyl ketone
MeOH	methanol
2-MeTHF	2-methyltetrahydrofuran
MFN	mitofusin
MTBE	methyl tert-butyl ether
NMR	nuclear magnetic resonance
PAMPA-BBB	passive artificial blood brain barrier membrane permeability assay
PBS	phosphate-buffered saline
PK	pharmacokinetic
PPH3	triphenylphosphine
r.t.	room temperature
SFC	supercritical fluid chromatography
TEA	triethylamine
THF	Tetrahydrofuran
tPSA	topological polar surface area

REFERENCES

1. Knott AB; Perkins G; Schwarzenbacher R; Bossy-Wetzel E Mitochondrial fragmentation in neurodegeneration. Nat. Rev. Neurosci 2008, 9, 505–518. [PubMed: 18568013]

2. Chan DC Fusion and fission: Interlinked processes critical for mitochondrial health. Annu. Rev. Genet 2012, 46, 265–287. [PubMed: 22934639]

3. Koshiba T; Detmer SA; Kaiser JT; Chen H; McCaffery JM; Chan DC Structural basis of mitochondrial tethering by mitofusin complexes. Science 2004, 305, 858–862. [PubMed: 15297672]

4. Chen H; Detmer SA; Ewald AJ; Griffin EE; Fraser SE; Chan DC Mitofusins mfn1 and mfn2 coordinately regulate mitochondrial fusion and are essential for embryonic development. J. Cell Biol 2003, 160, 189–200. [PubMed: 12527753]

5. Eura Y; Ishihara N; Yokota S; Mihara K Two mitofusin proteins, mammalian homologues of fzo, with distinct functions are both required for mitochondrial fusion. J. Biochem 2003, 134, 333–344. [PubMed: 14561718]

6. Dorn GW, 2nd. Evolving concepts of mitochondrial dynamics. Annu. Rev. Physiol 2019, 81, 1–17. [PubMed: 30256725]

7. Feely SM; Laura M; Siskind CE; Sottile S; Davis M; Gibbons VS; Reilly MM; Shy ME Mfn2 mutations cause severe phenotypes in most patients with cmt2a. Neurology 2011, 76, 1690–1696. [PubMed: 21508331]

8. Stuppia G; Rizzo F; Riboldi G; Del Bo R; Nizzardo M; Simone C; Comi GP; Bresolin N; Corti S Mfn2-related neuropathies: Clinical features, molecular pathogenesis and therapeutic perspectives. J. Neurol. Sci 2015, 356, 7–18. [PubMed: 26143526]

9. Wang L; Gao J; Liu J; Siedlak SL; Torres S; Fujioka H; Huntley ML; Jiang Y; Ji H; Yan T; Harland M; Termsarasab P; Zeng S; Jiang Z; Liang J; Perry G; Hoppel C; Zhang C; Li H; Wang X Mitofusin

2 regulates axonal transport of calpastatin to prevent neuromuscular synaptic elimination in skeletal muscles. Cell Metab 2018, 28, 400–414.e408. [PubMed: 30017354]

10. Kim J; Moody JP; Edgerly CK; Bordiuk OL; Cormier K; Smith K; Beal MF; Ferrante RJ Mitochondrial loss, dysfunction and altered dynamics in huntington's disease. Hum. Mol. Genet 2010, 19, 3919–3935. [PubMed: 20660112]

11. Zorzano A; Sebastian D; Segales J; Palacin M The molecular machinery of mitochondrial fusion and fission: An opportunity for drug discovery? Curr Opin Drug Discov Devel 2009, 12, 597–606.

12. Miret-Casals L; Sebastián D; Brea J; Rico-Leo EM; Palacín M; Fernández-Salguero PM; Loza MI; Albericio F; Zorzano A Identification of new activators of mitochondrial fusion reveals a link between mitochondrial morphology and pyrimidine metabolism. Cell Chem Biol 2018, 25, 268–278.e264. [PubMed: 29290623]

13. Wang D; Wang J; Bonamy GM; Meeusen S; Brusch RG; Turk C; Yang P; Schultz PG A small molecule promotes mitochondrial fusion in mammalian cells. Angew. Chem. Int. Ed. Engl 2012, 51, 9302–9305. [PubMed: 22907892]

14. Franco A; Kitsis RN; Fleischer JA; Gavathiotis E; Kornfeld OS; Gong G; Biris N; Benz A; Qvit N; Donnelly SK; Chen Y; Mennerick S; Hodgson L; Mochly-Rosen D; Dorn GW II. Correcting mitochondrial fusion by manipulating mitofusin conformations. Nature 2016, 540, 74–79. [PubMed: 27775718]

15. Rocha AG; Franco A; Krezel AM; Rumsey JM; Alberti JM; Knight WC; Biris N; Zacharioudakis E; Janetka JW; Baloh RH; Kitsis RN; Mochly-Rosen D; Townsend RR; Gavathiotis E; Dorn GW 2nd. Mfn2 agonists reverse mitochondrial defects in preclinical models of charcot-marie-tooth disease type 2a. Science 2018, 360, 336–341. [PubMed: 29674596]

16. Dang X; Zhang L; Franco A; Li J; Rocha AG; Devanathan S; Dolle RE; Bernstein PR; Dorn GW, 2nd. Discovery of 6-phenylhexanamide derivatives as potent stereoselective mitofusin activators for the treatment of mitochondrial diseases. J. Med. Chem 2020, 63, 7033–7051. [PubMed: 32506913]

17. Franco A; Dang X; Walton EK; Ho JN; Zablocka B; Ly C; Miller TM; Baloh RH; Shy ME; Yoo AS; Dorn GW 2nd. Burst mitofusin activation reverses neuromuscular dysfunction in murine cmt2a. Elife 2020, 9.

18. Yan L; Huo P; Hale JJ; Mills SG; Hajdu R; Keohane CA; Rosenbach MJ; Milligan JA; Shei GJ; Chrebet G; Bergstrom J; Card D; Mandala SM Sar studies of 3-arylpropionic acids as potent and selective agonists of sphingosine-1-phosphate receptor-1 (s1p1) with enhanced pharmacokinetic properties. Bioorg. Med. Chem. Lett 2007, 17, 828–831. [PubMed: 17092714]

19. Thorarensen A; Wakefield BD; Romero DL; Marotti KR; Sweeney MT; Zurenko GE; Rohrer DC; Han F; Bryant GL Jr. Preparation of novel anthranilic acids as antibacterial agents. Extensive evaluation of alternative amide bioisosteres connecting the a- and the b-rings. Bioorg. Med. Chem. Lett 2007, 17, 2823–2827. [PubMed: 17368020]

20. Shiozaki M; Maeda K; Miura T; Ogoshi Y; Haas J; Fryer AM; Laird ER; Littmann NM; Andrews SW; Josey JA; Mimura T; Shinozaki Y; Yoshiuchi H; Inaba T Novel n-substituted 2-phenyl-1-sulfonylamino-cyclopropane carboxylates as selective adamts-5 (aggrecanase-2) inhibitors. Bioorg. Med. Chem. Lett 2009, 19, 1575–1580. [PubMed: 19243944]

21. Talele TT The "cyclopropyl fragment" is a versatile player that frequently appears in preclinical/clinical drug molecules. J. Med. Chem 2016, 59, 8712–8756. [PubMed: 27299736]

22. Poduslo JF; Curran GL; Berg CT Macromolecular permeability across the blood-nerve and blood-brain barriers. Proc. Natl. Acad. Sci. U. S. A 1994, 91, 5705–5709. [PubMed: 8202551]

23. Reinhold AK; Rittner HL Characteristics of the nerve barrier and the blood dorsal root ganglion barrier in health and disease. Exp. Neurol 2020, 327, 113244. [PubMed: 32057794]

24. Heiman-Patterson TD; Deitch JS; Blankenhorn EP; Erwin KL; Perreault MJ; Alexander BK; Byers N; Toman I; Alexander GM Background and gender effects on survival in the tgn(sod1-g93a)1gur mouse model of als. J. Neurol. Sci 2005, 236, 1–7. [PubMed: 16024047]

25. Guyenet SJ; Furrer SA; Damian VM; Baughan TD; La Spada AR; Garden GA A simple composite phenotype scoring system for evaluating mouse models of cerebellar ataxia. J Vis Exp 2010.

26. Misko A; Jiang S; Wegorzewska I; Milbrandt J; Baloh RH Mitofusin 2 is necessary for transport of axonal mitochondria and interacts with the miro/milton complex. J. Neurosci 2010, 30, 4232–4240. [PubMed: 20335458]

27. Kruppa AJ; Buss F Motor proteins at the mitochondria-cytoskeleton interface. J. Cell Sci 2021, 134.

28. Dorn GW 2nd. Mitofusins as mitochondrial anchors and tethers. J. Mol. Cell. Cardiol 2020, 142, 146–153. [PubMed: 32304672]

29. Lacivita E; Niso M; Mastromarino M; Garcia Silva A; Resch C; Zeug A; Loza MI; Castro M; Ponimaskin E; Leopoldo M Knowledge-based design of long-chain arylpiperazine derivatives targeting multiple serotonin receptors as potential candidates for treatment of autism spectrum disorder. ACS Chem. Neurosci 2021, 12, 1313–1327. [PubMed: 33792287]

24. ldrick GM; SHELXTL-2014, Crystallographic Computing System; Bruker Analytical X-Ray Instruments: Madison, WI, 2014

25. Sheldrick GM; A short history of SHELX; Acta. Cryst. A, 2008, A64, 112–122
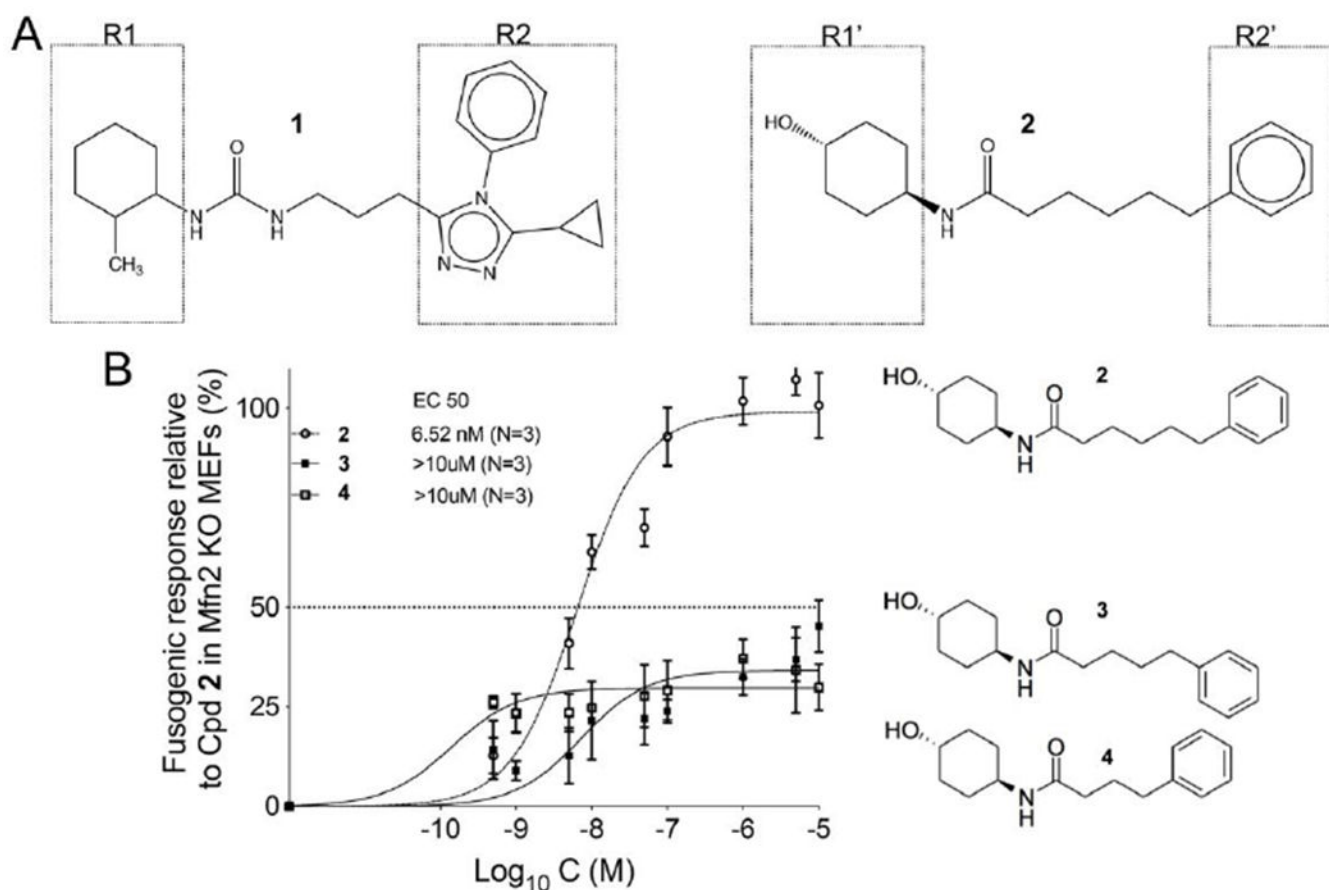
Figure 1. Structures of triazolurea (1) and phenylhexanamide (2) mitofusin activators.
A. Both classes of mitofusin activator share a substituted cyclohexyl (R1, R1') linked to
an aromatic moiety (R2, R2') by a six or seven member alkyl linker. **B.** Dose-response
relationships for mitochondrial elongation (measured as the increase in mitochondrial aspect
ratio) of **2** and its analogs having one (**3**) or two (**4**) fewer carbons in the alkyl linker.

2

MW-289.2; log p-3.717; HBD-2; HBA-3;
CNS MPO-5.0

5

MW-301.2; log p-3.609; HBD-2; HBA-3;
CNS MPO-5.1

6

MW-301.2; log p-3.824; HBD-2; HBA-3;
CNS MPO-5.1

7

MW-301.2; log p-3.824; HBD-2; HBA-3;
CNS MPO-5.0

8

MW-301.2; log p-3.824; HBD-2; HBA-3;
CNS MPO-5.0

9

MW-288.01; log p-4.178; HBD-2; HBA-3;
CNS MPO-4.7

10

MW-300.01; log p-4.747; HBD-2; HBA-3;
CNS MPO-4.4

11

MW-300.01; log p-4.747; HBD-2; HBA-3;
CNS MPO-4.4

12

MW-300.01; log p-4.747; HBD-2; HBA-3;
CNS MPO-4.4

13

MW-288.01; log p-4.178; HBD-2; HBA-3;
CNS MPO-4.7

Figure 2. Designs for variants of 2 having cycloalkyl linkers.
Calculated Lipinski Rule values and central nervous system multiparameter optimization
desirability (MPO) factors are shown below. MW = molecular weight; log p = octanol-water
partition coefficient; HBD = number of hydrogen bond donors; HBA = number of hydrogen
bond acceptors.
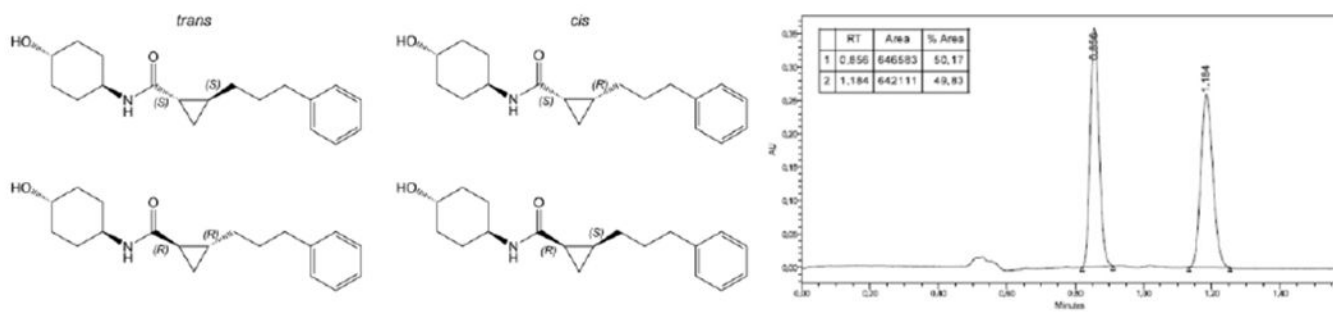
Figure 3. Synthesis of 5 results in a ~50:50 mixture of 5 trans- stereoisomers.

Left, structures of the four possible **5** stereoisomers. *Right*, chiral separation identifies two forms, shown to be *trans-* based on ^{1}H-NMR of synthetic intermediate **5C** (Figure S2).
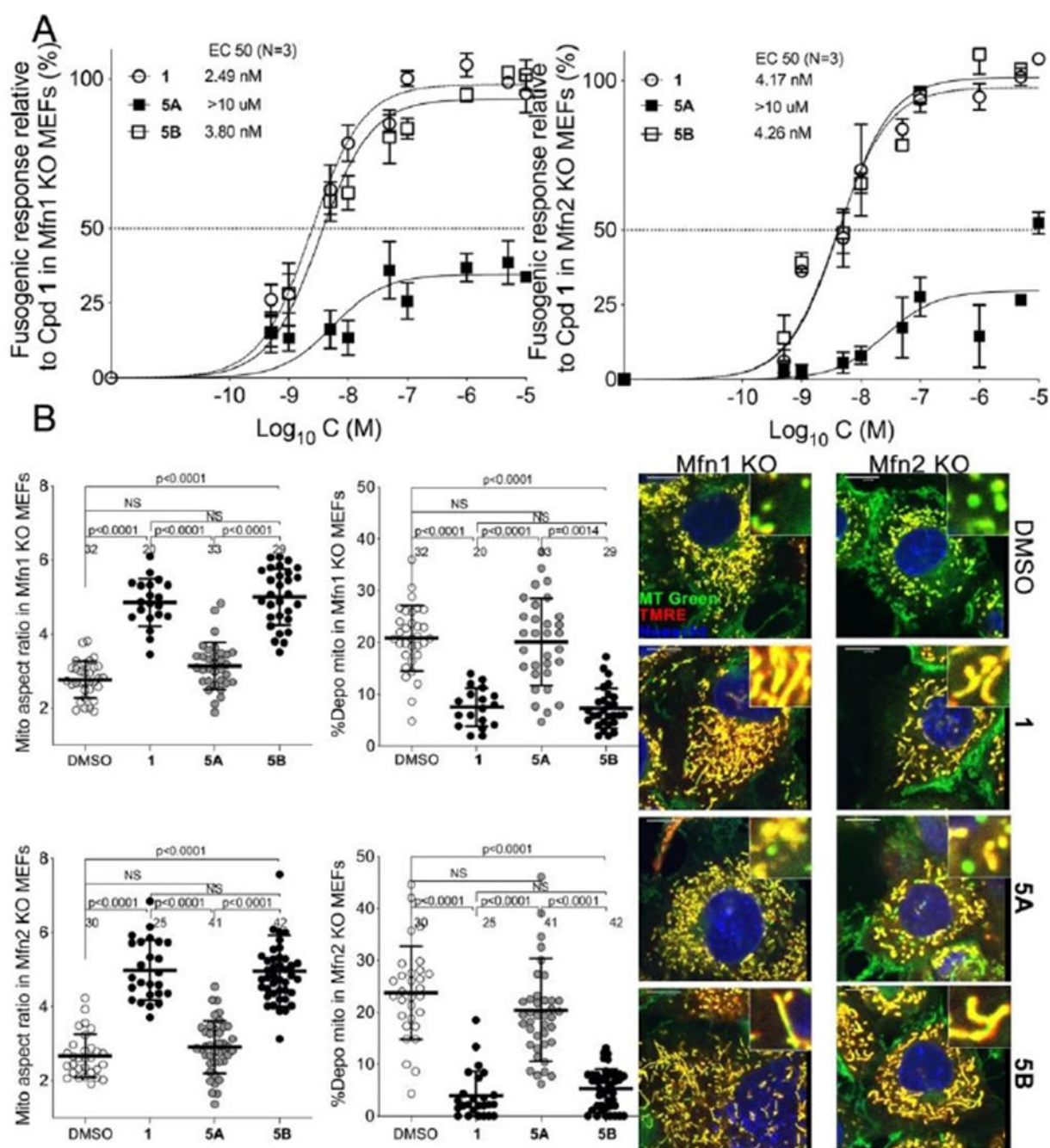
Figure 4. Mitochondrial elongation and polarization-enhancing activities of 5 enantiomers.
A. Dose-response curves for **5A** and **5B** to increase mitochondrial aspect ratio (length/width) in cultured fibroblasts lacking Mfn1 (left, **5A**: $EC_{50} > 10\mu M$, **5B**: $EC_{50} = 3.80nM$; 95% confidence limits, 2.70-5.28nM) or Mfn2 (right, **5A**: $EC_{50} > 10\mu M$, **5B**: $EC_{50} = 4.26nM$; 95% confidence limits, 2.99-6.04nM). Parallel studies with prototype mitofusin activator **1** are shown for comparison. *B*. Group data (left) and representative live cell confocal micrographs (right) from Mfn1 and Mfn2 null cells showing mitochondrial elongation (increase in aspect ratio) and reversal of depolarization with 1 µM test compound

added for 48 hours. Enlarged mitochondria are shown in *insets*. Mitochondria staining yellow are highly polarized, i.e. healthy; green staining mitochondria are depolarized and dysfunctional.
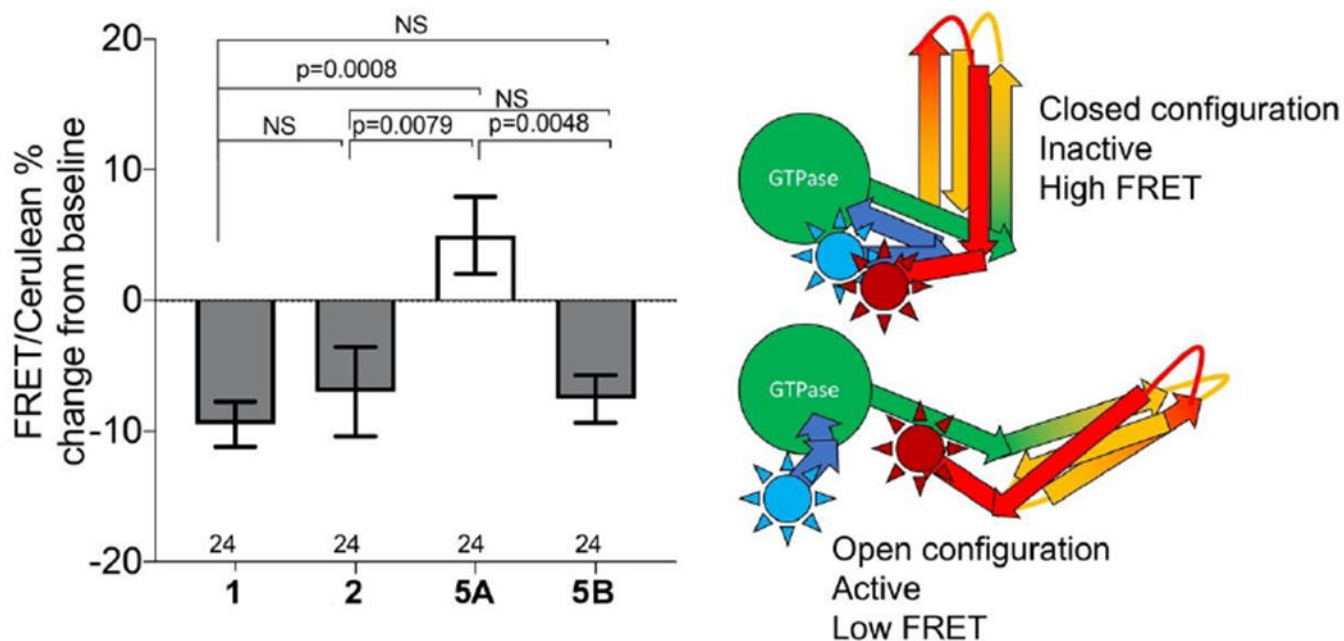
Figure 5. MFN2 altering activity of 5 is stereoisomer-specific.
Results of FRET studies comparing MFN2 conformation altering activities of prototype mitofusin activators **1** and **2** with **5** stereoisomers (all compounds added to a final concentration of 1μM as in Figure 4B; assays were performed after 4 hours). Decreased FRET signal reflects MFN2 unfolding as depicted to the right. Blue sun indicates position of amino terminal mCerulean; red sun is C-terminal mVenus. Means ± SEM of 6 separate studies with 4-6 replicates each.
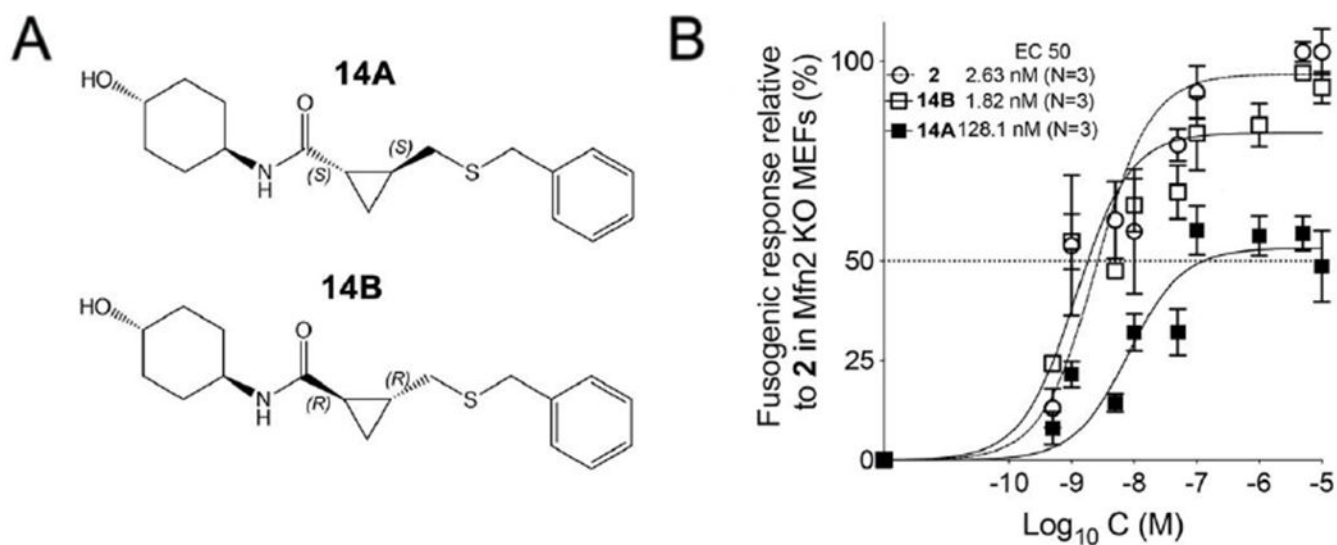
Figure 6. Mitochondrial fusogenic activities of 5 sulfide analogs.
A. Structures of **5** sulfide analogs synthesized for X-ray diffraction studies. **B.** Dose-response curves showing **14B** (slower eluting isoform: EC_{50} = 1.82 nM; 95% confidence limits, 1.04-2.99 nM) and **14A** (faster eluting isoform: EC_{50} = 128.1 nM; 95% confidence limits, 141.94~ nM) increasing mitochondrial aspect ratio (length/width) in cultured fibroblasts lacking Mfn2. Data are means ± SEM from three independent experiments. **1** dose-response is shown for comparison (EC_{50} = 2.63 nM; 95% confidence limits, 1.45-4.64 nM).
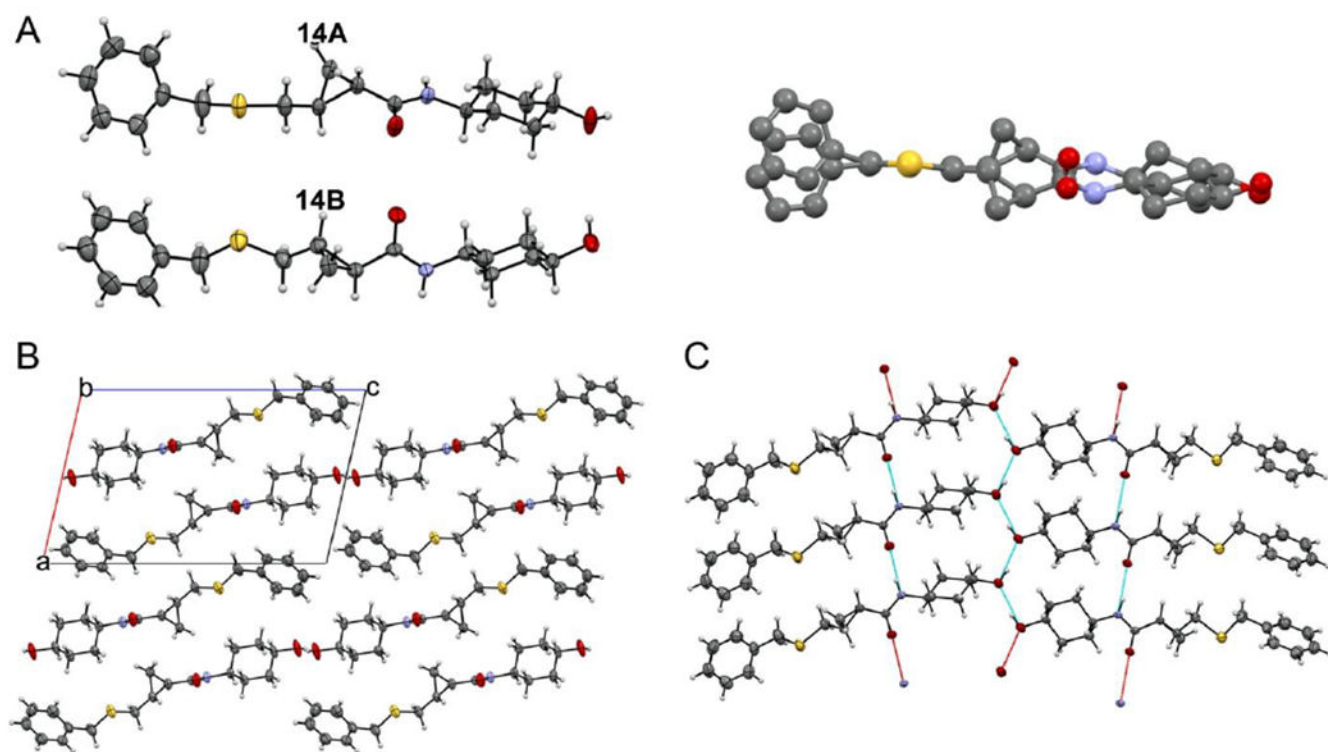
Figure 7. SCXRD structures of 14A and 14B.
A. (left) ORTEP diagrams of **14A** (inactive) and **14B** (active). Thermal ellipsoids are shown at 50% confidence intervals. Hydrogen atoms are geometrically idealized. (right) Superposition of **14A** and **14B** showing mirror structures. Hydrogen atoms are omitted for clarity **B.** Packing diagram viewed along the b-axis. Unit cell axes are shown and labeled. **C.** Hydrogen-bonding interactions for **14B**. Complete hydrogen bonds are shown in blue; red bonds indicate that only one participating atom is present in the pictured molecules.
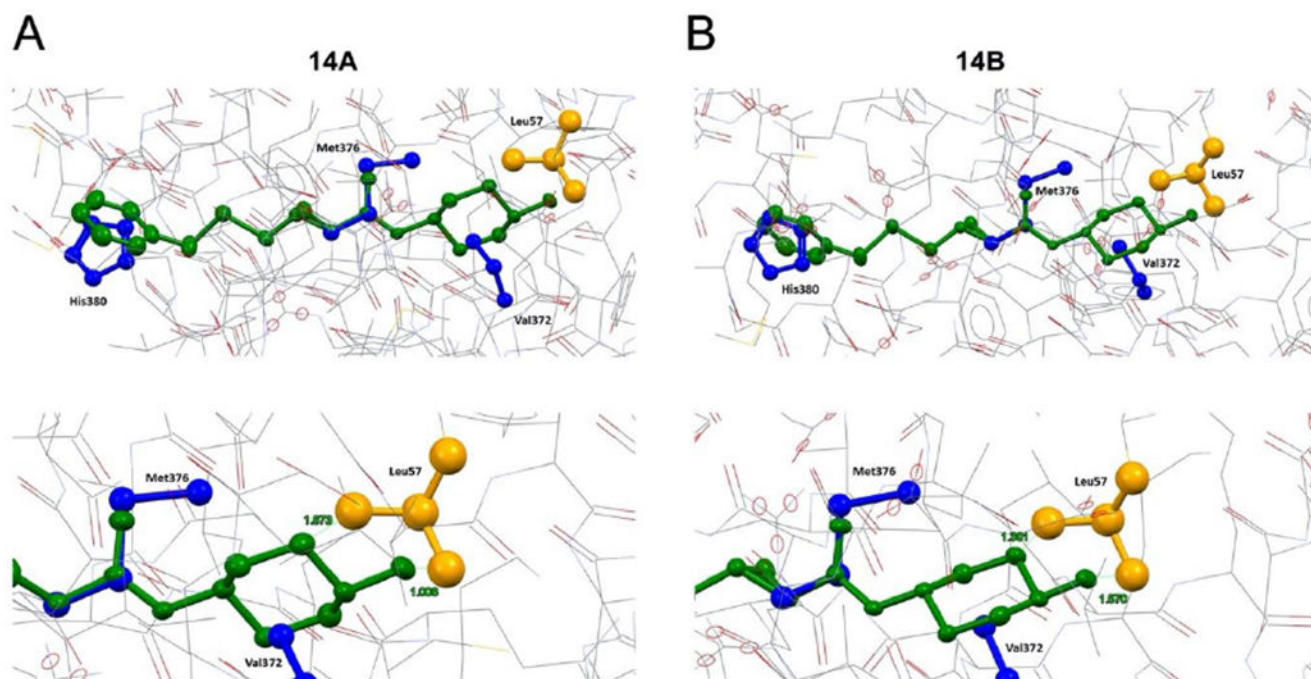
Figure 8. MFN2 peptide mimicry of 5 sulfide analog enantiomers.
(*top*) Superimposition of compound. enantiomers (**A**, **14A**, **B**, **14B**; both are green) onto human MFN2 residues Val372, Met376 and His380 (blue) modeled as shown in Figure S5. MFN2 Leu57 is shown in orange. (*bottom*) Close-up of modeled interactions between compound enantiomers and MFN2 Leu57. Human Mfn2 protein structure was computationally modeled in closed configuration based on structural homology with human Mfn1 (PDB ID: 5GNS) and Arabidopsis thaliana dynamin-related protein (PDB ID: 3T34).
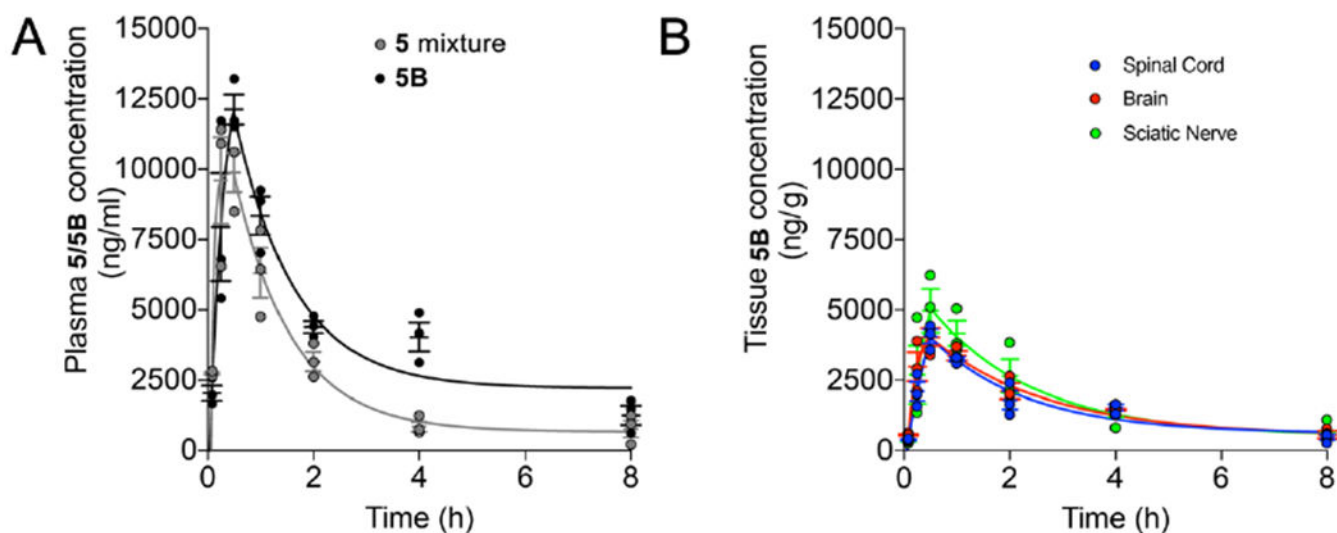
Figure 9. Plasma and tissue pharmacokinetics of 5B after oral administration to non-fasted mice.
A. Plasma pharmacokinetics of **5** isomeric mixture vs **5B** in mice after a single oral dose of 50 mg/kg. **B.** Comparative neuronal tissue concentrations of **5B** after a single oral dose of 50 mg/kg. Vertical axis values are the same in **A** and **B**. Data are means ± SEM, each dot represents one mouse. Calculated values are in the text.
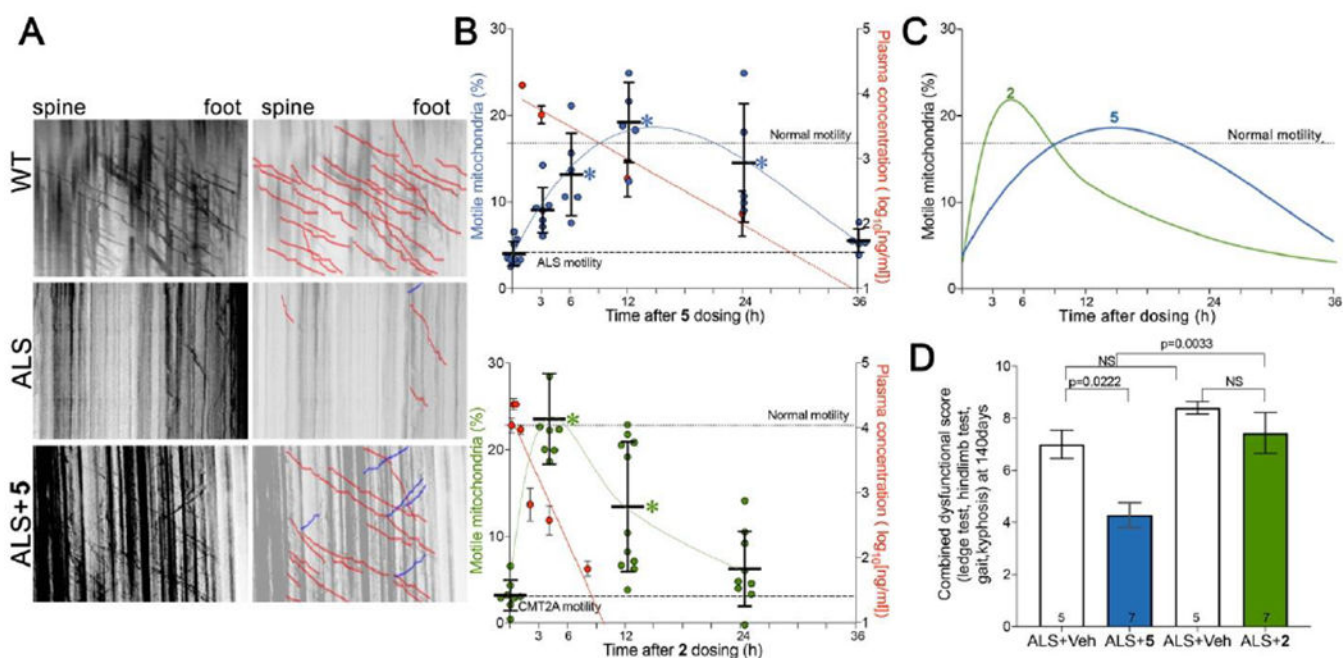
Figure 10.
Pharmacodynamic and therapeutic effects *of 5 vs 2 in murine ALS.* **A.** Representative kymographs for wild-type (WT) and ALS SOD1G93A mice (ALS) 12 hours after oral administration of **5** or vehicle. **B.** Time-dependent pharmacokinetics/pharmacodynamics of **5** and **2** after single oral doses (60 mg/kg). (top) Blue values and left vertical axis show mitochondrial motility after **5** in ALS mouse sciatic nerve axons. (bottom) green values and left vertical axis show mitochondrial motility in CMT2A mouse sciatic nerve axons. Each point represents a single neuronal axon, from two or three mice per time point. Red values and right vertical axes of top graph show corresponding plasma **5** levels (n=5 per time point; means ± SD); plasma levels of **2** are from ([17]). Dotted line designated "Normal motility" is mean value for WT in panel **A**; dashed line designated "ALS motility" is mean value for untreated ALS in panel **A**. **C.** Comparative pharmacodynamics of **5** (blue) and **2** (green). **D.** Effects of **5** (blue) and **2** (green) on neuromuscular dysfunction score (ledge test, hindlimb test, gait, kyphosis; [25]) in a proof-of-concept study of ALS mice. P values by ANOVA.
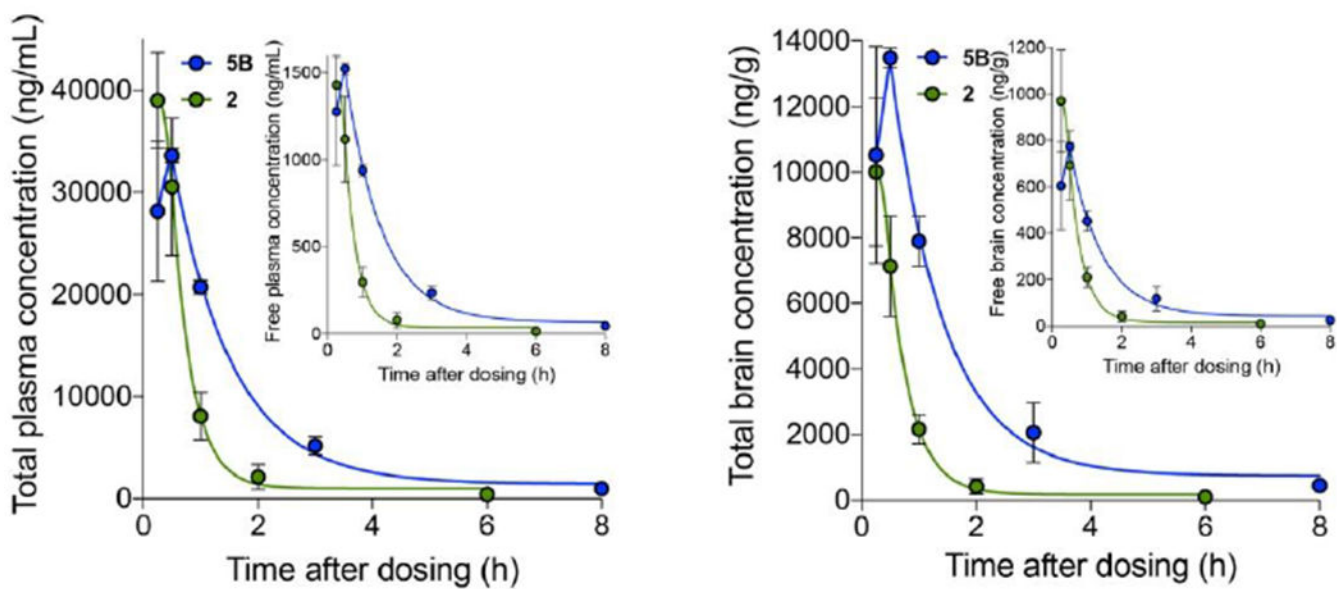
Figure 11. Comparative pharmacokinetic properties of 5B and 2 in fasted mice.
Left panel, total compound levels in plasma for **2** (green) and **5B** (blue); inset shows free concentrations. **Right panel**, total brain compound levels; inset shows free concentrations. Means±SEM of three mice per time point. Calculated values are in Table 4.
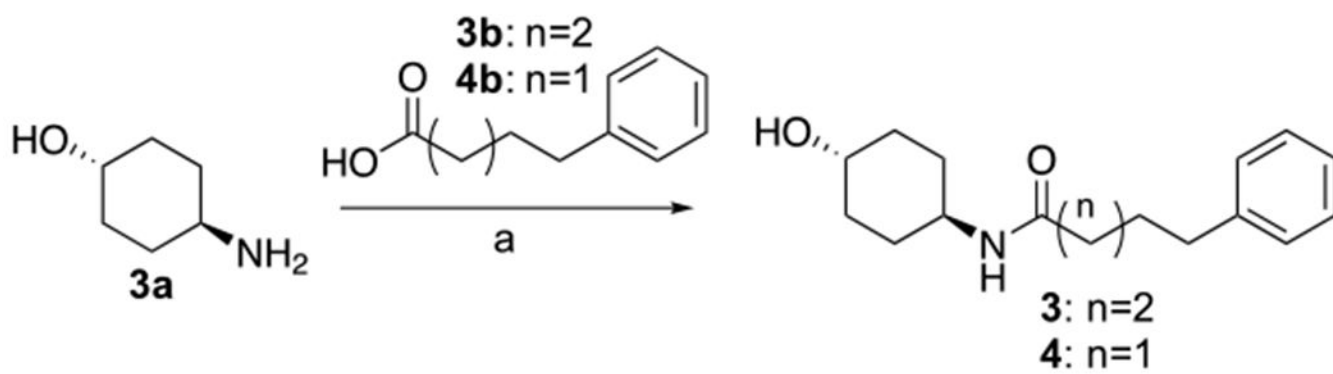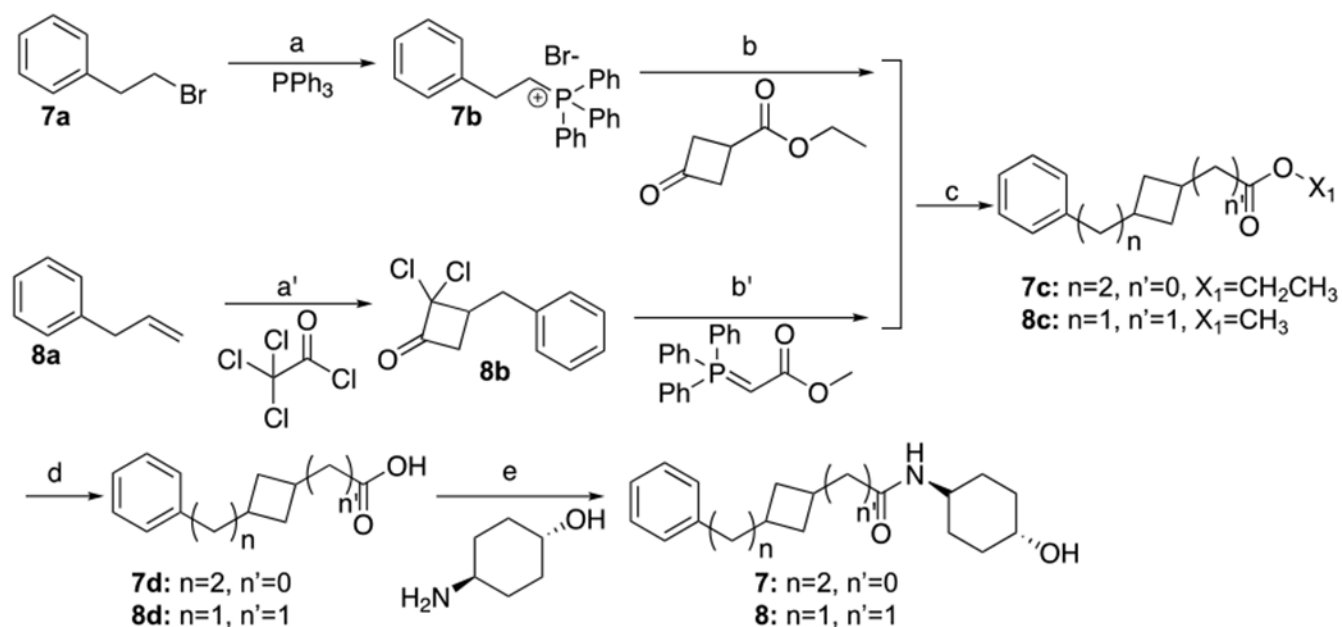
Scheme 1.

Synthesis of **3**, **4**[a]

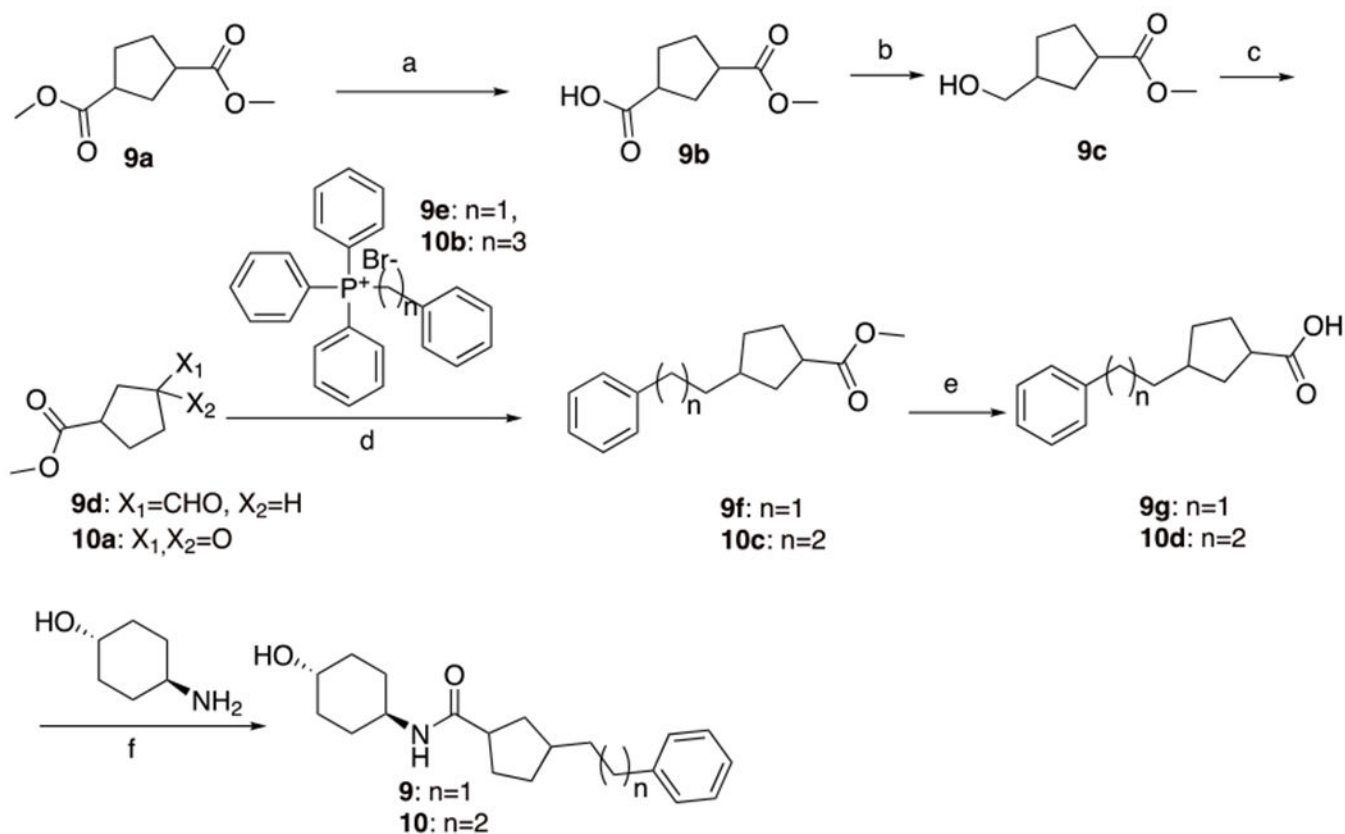[a]Reagents and conditions: HATU, Et$_3$N, THF, 25°C, 2h.
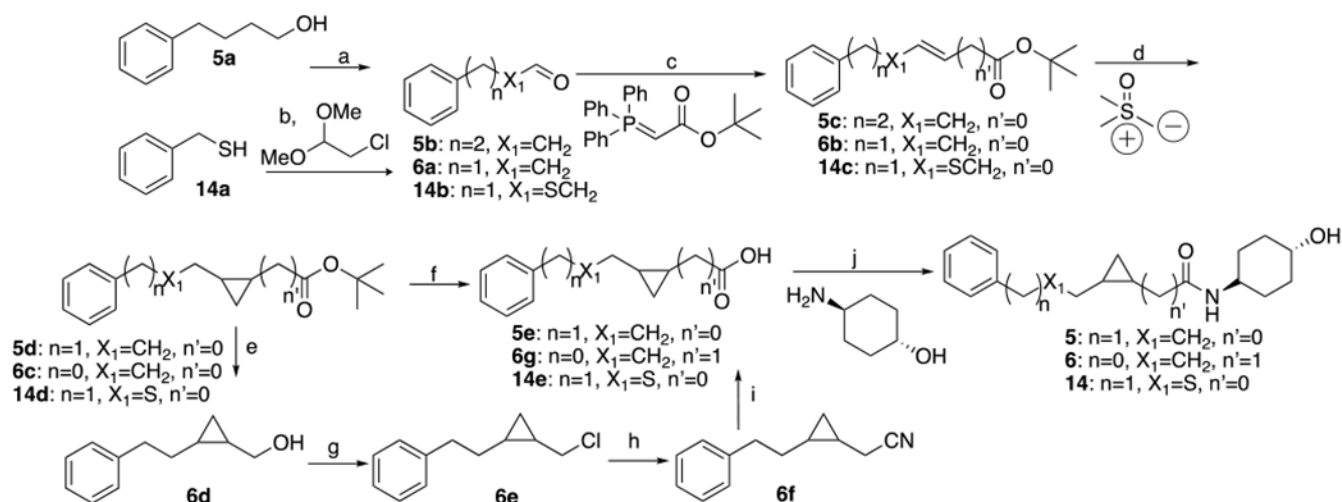
Scheme 2.
Synthesis of **5, 6 and 14**[a]

[a]Reagents and conditions: (a) oxalyl chloride, DMSO, TEA, DCM, −55-25°C, 20min. (b) i. EtOH, EtONa, KI; ii. 2-chloro-1,1-dimethoxyethane, 80°C, 12h; H_2O, H_2SO_4, 60°C, 12h. (c) THF, 20°C. **5, 14** : 12h, **6**: 1h. (d) NaH, DMSO, 20°C, 1.5h. (e) $LiAlH_4$, THF, 0-25°C, 3h. (f) TFA, DCM, 25°C, 15h. (g) $SOCl_2$, TEA, $CHCl_3$, 0-70°C, 1h. (h) N(nBu)$_4$CN, THF, 70°C, 12h. (i) KOH, EtOH, H_2O, 100°C, 16h. (j) HOBt, EDCI, DIEA, DMV, 25°C. **5, 6**: 16h, **14**: 2h.

Scheme 3.

Synthesis of **7** and **8**[a]

[a]Reagents and conditions: (a) 100°C, 16h. (b) sodium 2-methybutan-2-olate, toluene, 20-70°C, 4.5h. (a') zinc-copper couple, Et$_2$O, 20-35°C, 18h. (b') acetic acid, zinc, 25-80°C, 3h, toluene, 110°C, 2h. (c) H2, Pd/C. **7:** EtOH, 20°C, 16h. **8:** MeOH, 25°C 2h. (d) LiOH•H$_2$O, MeOH/THF/H$_2$O. **7:** 20°C, 2h. **8:** 25°C, 16h. (e) HOBt, EDCI, DIPEA, DMF, 16h. **7**: 20°C, **8:** 25°C.
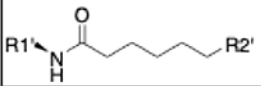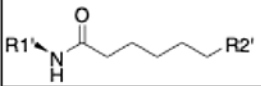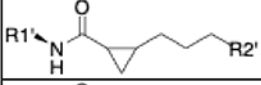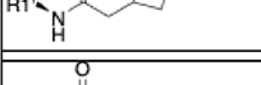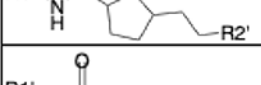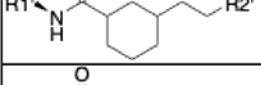
Scheme 4.
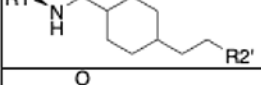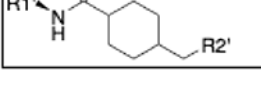Synthesis of **9** and **10**[a]

[a]Reagents and conditions: (a) NaOH, MeOH, 25°C, 12h. (b) BH$_3$-Me$_2$S, THF, −78-25°C, 12.5h. (c) Dess-Martin, DCM, 25°C, 2h. (d) i. t-BuOK, **9**: −20°C, 2h. **10**: toluene, 70°C, 17h. ii. Pd/C, H$_2$, MeOH, 25°C, **9**: 2h, **10**: 4h. (e) LiOH•H$_2$O, MeOH, THF, H$_2$O, **9**: 25-70°C, 2h, **10**: 70°C, 3h. (f) HATU, Et$_3$N, THF, 25°C, **9**: 12h, **10**: 16h.
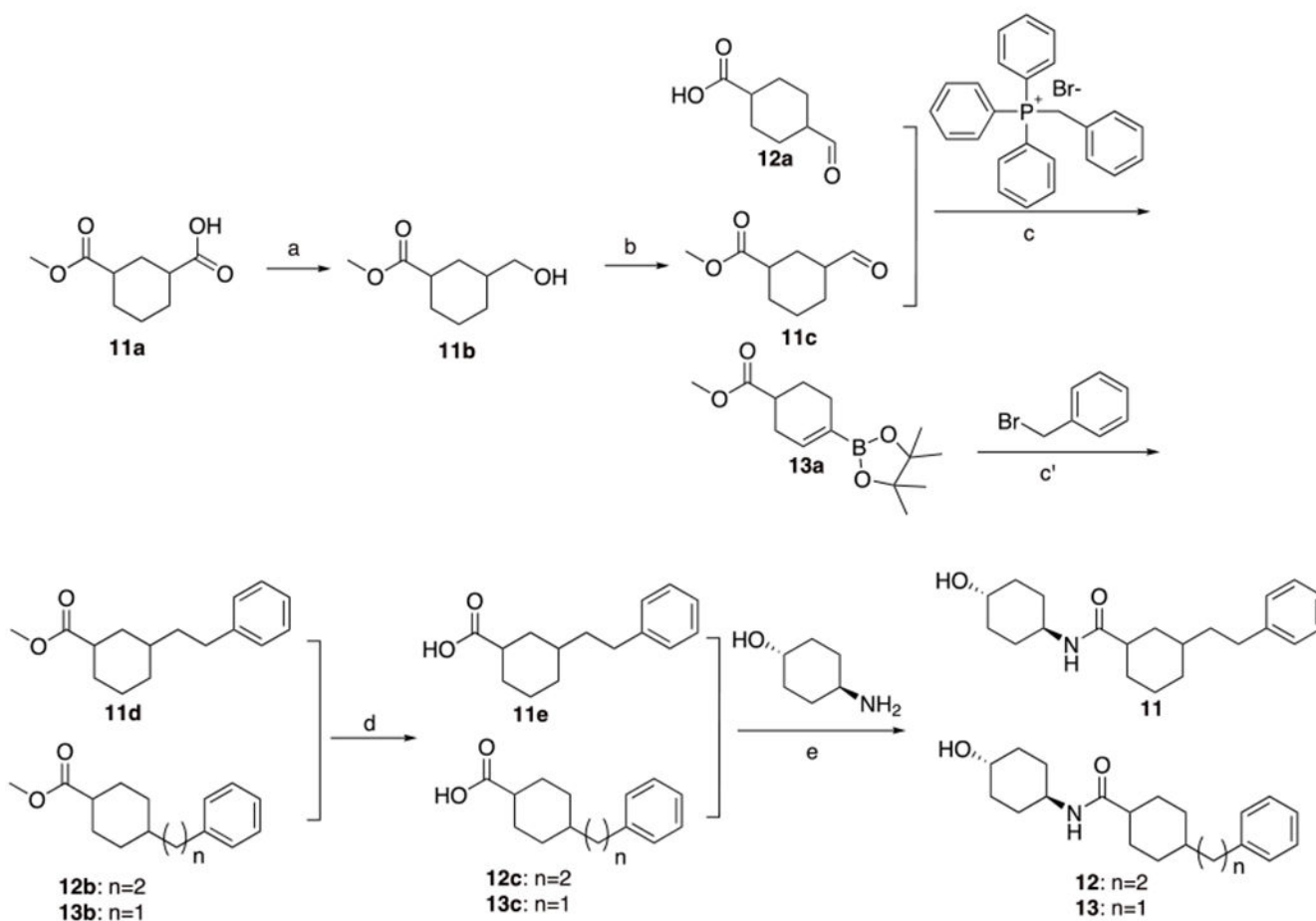
Scheme 5.

Synthesis of **11, 12** and **13**[a]

[a]Reagents and conditions: (a) BH$_3$-SMe$_2$, THF, −78-25°C, 12.5h. (b) pyridine sulfur trioxide, Et$_3$N, DMSO, 25°C, 12h. (c) i. THF, t-BuOK, N$_2$, −20°C, 2h, ii. Pd/C, H$_2$, MeOH, 25°C, 2h. (c') i. Pd(dppf)Cl$_2$, dioxane, H$_2$O, K$_2$CO$_3$, N$_2$, 25-100°C, 2h. ii. Pd/C, H$_2$, MeOH, 25°C, 2h. (d) LiOH•H$_2$O, MeOH, THF, H$_2$O, 25-70°C, 2h. (e) HATU, Et$_3$N, THF, 25°C, 12h.

Table 1.

Functional and pharmacokinetic properties of cycloalkyl linker 2 variants [a].

		EC50 (nM)	Plasma Protein Binding (% Bound)		Liver Microsomes (t1/2, min)		PAMPA (Pe, 10^-6 cm/s)
			human	mouse	human	mouse	
	2	5.8	91	96.3	>145	92.4	26
	5	5.1	94.4	95.5	>145	114.1	58
	6	5.6	89.1	93.1	>145	76.7	39
	7	11	97.2	94.3	>145	105.5	61
	8	85	95.3	93.5	>145	124.9	37
	9	7	97.73	95.97	>145	35.1	114
	10	15.3	99.25	98.8	120.2	43.2	154
	11	4.8	97.77	4.03	69.2	20.5	126
	12	7.4	99.59	98.86	>145	74.4	133
	13	44.6	92.05	94.43	>145	49.3	88.8

[a] Linker modifications of **2** are shown to the left; functional and PK characteristics are to the right. R1' is cyclohexanol and R2' is phenyl as in Figure 1. EC50 95% confidence limits are shown in Figure S1.

Table 2.

In vivo pharmacokinetic properties of **5** ^{a}.

	5		2
Dose (mg/kg)	10		10
C_0 (ng/mL)	32111		50,600
$t_{1/2}$ (hours)	1.64		1.1
$AUC_{0\text{-last}}$ (ng*h/mL)	9178		11495
Vdss (L/kg)	0.6		0.347

^{a}IV administration in mice, 10 mg/kg; values for **2** are from ([16]).

Table 3.

Pharmacokinetic properties of 5B in plasma and nerve tissue [a].

Compound	Tissue	Dose Route	Actual Mean Dosage (mg/kg)	$t_{1/2}$ (h)	t_{max} (h)	C_{max} (ng/mL)	AUC_{last} (h*ng/mL)	MRT_{inf} (h)
5B	Plasma	PO	50	2.83	0.50	12100	34000	3.96
	Brain	PO	50	3.13	0.50	4030	13400	4.30
	Spinal Cord	PO	50	2.71	0.50	4060	12700	3.93
	Left Sciatic Nerve	PO	50	3.21	0.50	4570	15300	4.62
	Right Sciatic Nerve	PO	50	2.61	0.50	5370	13800	3.35

[a] Studies were performed in non-fasted mice, resulting in lower plasma **5B** levels than reported after the same oral dose in fasted mice (see Table 4).

Table 4.

Comparative plasma and brain pharmacokinetic properties of parent 2 and lead compound 5B in fasting mice [a].

	Cpd 2 (50 mg/kg PO)		Cpd 5B (50 mg/kg PO)	
	total Plasma	free Plasma	total Plasma	free Plasma
C_{max} (ng/mL)	39011	1428	33619	1523
$T_{1/2}$ (h)	1.280		1.67	
AUC_{0-last} (ng.h/mL)	30612	1121	59567	2697
MRT_{0-last} (h)	1.01		1.92	
	total Plasma	free Plasma	total Plasma	free Plasma
C_{max} (ng/g)	10001	970	13480	774
$T_{1/2}$ (h)	0.999		1.77	
AUC_{0-last} (ng.h/g)	7392	717	23465	1347
MRT_{0-last} (h)	0.959		1.98	

[a] Free compound concentrations were calculated from protein binding assays: **2** – mouse plasma 96.7%, mouse brain 90.3%; **5B** – mouse plasma 95.5%, mouse brain 94.3%.